Licentiate Thesis in Physics

Multi-messenger emission from gamma-ray bursts

Filip Samuelsson

Particle and Astroparticle Physics, Department of Physics,
Royal Institute of Technology, SE-106 91 Stockholm, Sweden

Stockholm, Sweden 2020

Cover illustration: Artistic expression of a gamma-ray burst made by Angelica Alamaa.

Akademisk avhandling som med tillstånd av Kungliga Tekniska högskolan i Stockholm framlägges till offentlig granskning för avläggande av teknologie licentiatexamen onsdagen den 10 juni 2020 kl 15:15 i sal A5:1003, AlbaNova Universitetscentrum, Roslagstullsbacken 21, Stockholm.

Avhandlingen försvaras på engelska.

ISBN 978-91-7873-560-0
TRITA-SCI-FOU 2020:20

Printed by Universitetsservice US-AB

Abstract

Multi-messenger astronomy is a very hot topic in the astrophysical community. A messenger is something that carries information. Different astrophysical messenger types are photons, cosmic rays, neutrinos, and gravitation waves. They all carry unique and complementary information to one another. The idea with multi-messenger astronomy is that the more different types of messengers one can obtain from the same event, the more complete the physical picture becomes.

In this thesis I study the multi-messenger emission from gamma-ray bursts (GRBs), the most luminous events known in the Universe. Specifically, I study the connection of to extremely energetic particles called ultra-high-energy cosmic rays (UHECRs). UHECRs have unknown origin despite extensive research. GRBs have long been one of the best candidates for the acceleration of these particles but a firm connection is yet to be made. In Paper I and Paper II, we study the possible GRB-UHECR connection by looking at the electromagnetic radiation from electrons that would also accelerated together with the UHECR. My conclusion is that the signal from these electrons does not match current GRB observation, disfavoring that a majority of UHECRs comes from GRBs.

Sammanfattning

”Multi-messenger astronomy” (mångbudbärarastronomi, fri översättning) är ett väldigt aktuellt område inom astrofysiken just nu. En meddelare är någonting som bär på information. Olika meddelartyper inom astrofysiken är fotoner, kosmisk strålning, neutriner och gravitations vågor. Dessa har alla unik och olika typ av information som kompletterar varandra. Idén bakom multi-meddelare-astronomi är att ju fler olika meddelartyper vi kan upptäcka från samma event, desto mer komplett blir vår fysikaliska tolkning.

I denna avhandling studerar jag multi-meddelare emission från gammablixtar (GRBs), de mest ljusstarka företeelser vi känner till i Universum. Mer specifikt, såstuderar jag kopplingen mellan GRBs och ultraenergetisk kosmisk strålning (UHECRs). Ursprunget till UHECRs är fortfarande okänt trots långt pågående forskning. GRBs har länge varit en av de mest lovande accelerationskandidaterna men än sålänge finns inga fasta bevis. I Paper I och Paper II studerar vi den möjliga GRB-UHECR kopplingen genom att studera den elektromagnetiska strålningen från elektronerna som även de skulle bli accelererade tillsammans med UHECRs. Min slutsats är att strålningen från elektronerna inte matchar observationer från GRBs, vilket talar emot att en majoritet av UHECRs kommer från GRBs.

List of Publications

Publications Included in the Thesis

Paper I

The Limited Contribution of Low- and High-luminosity Gamma-Ray Bursts to Ultra- high-energy Cosmic Rays
Samuelsson, Filip; Bégué, Damien; Ryde, Felix; Pe'er, Asaf
The Astrophysical Journal, Volume 876, Issue 2, Article id. 93, 17 pp. (2019)
DOI: doi.org/10.3847/1538-4357/ab153c

Author's contribution: The idea behind the paper was thought of by Damien Bégué, Felix Ryde, and myself. I wrote all of the text in the article. I generated all figures and made all calculations, which were double checked by Damien Bégué. Throughout the development of the paper, all co-authors were involved in continuous discussion. All co-authors helped proof-read the manuscript several times, which heavily influenced and improved the manuscript.

Paper II

Constraining Low-luminosity Gamma-Ray Bursts as Ultra-high-energy Cosmic Ray Sources Using GRB 060218 as a Proxy
Samuelsson, Filip; Bégué, Damien; Ryde, Felix; Pe'er, Asaf; Kohta, Murase
Manuscript submitted to The Astrophysical Journal
arXiv identifier: 2005.02417

Author's contribution: The paper is a continuation of Paper I and the discussions with Kohta Murase that followed the publication of Paper I. I wrote all of the text. All figures are generated by me. The code used in the afterglow scenario is written by Asaf Pe'er. The continuous discussion between all co-authors helped shape and re-shape the paper. All co-authors helped proof-read the manuscript several times.

Contents

Chapter 1

Introduction

1.1 Multi-messenger astronomy

Originally, astronomy was centered only around what we were able to see with our own eyes. That changed in 1609 when Galileo Galilei managed to build a telescope, improving upon existing designs. With this new tool, the things astronomers were able to see and study greatly improved. However, all discoveries still relied solely on optical data.

Today, we obtain information from astrophysical events through many different channels. Observations are made all across the electromagnetic spectrum, even though optical observations are still of central importance. From low-energy radio observations with gigantic discs tens of meters across to high-energy gamma-ray observations made by space-borne satellites, all parts of the electromagnetic spectrum contributes differently to our knowledge of astrophysical events. Cosmic rays (CRs), high-energy charged particles, have been observed and studied for a century (Wulf, 1910; Hess, 1912). More recently, the detection of astrophysical neutrinos and gravitational waves have further completed our understanding. In astronomy, these different detection channels are referred to as different *messenger* types, because they carry unique and complementary information to one another. *Multi-messenger astronomy* is the term coined for astronomy done by observing several messenger types from the same event (Mészáros et al., 2019).

The advent of multi-messenger astronomy is a recent one. The first multi-messenger event was the famous supernova SN 1987A. A burst of neutrinos was detected in several contemporary neutrino experiments followed by a detection of a very bright supernova (SN) roughly two hours later (Arnett et al., 1989). The discovery was part of the Nobel Prize in physics

in 2002 (Nobel Media AB, 2002). In August of 2017, the ground breaking gravitational wave event GW 170817 was detected. 1.7 seconds later, the *Fermi*-satellite discovered a flash of gamma-rays, a so-called gamma-ray burst (GRB). The famous paper revealing the multi-messenger discovery has almost 3800 authors, over 1300 citations to date, and was named scientific discovery of the year (Abbott et al., 2017b). Most recently a high-energy neutrino was discovered in spatial and temporal coincidence to a flaring blazar, a black hole in the center of a galaxy that has a jet pointing towards us (IceCube Collaboration et al., 2018b,a). This event prompted a press conference by the National Science Foundation (National Science Foundation, 2018).

As evident from the discussion above, multi-messenger detections are always a big thing when they occur. Given that they are so valuable, how come that they are still so rare? First, the size of the Universe is problematic. Our enormous Universe makes even the intrinsically brightest events very dim when observed from Earth. Therefore, giant telescopes are needed and they must be pointed at the correct patch of the sky. Secondly, the timescale of the events involved are very short. When a satellite triggers on a signal, it first runs some automated tests to make sure it is something genuinely interesting and not just background noise. If deemed interesting enough, it determines the most likely position of the sky the signal came from and relays that information to other observatories. Once that information has been received, the ground-based observatories need to decide whether they think the signal is interesting or not. If it is decided that the signal is worthy of a follow-up observation, then and only then can the telescopes start to slew their large discs to the correct patch of the sky. Optimally, all of this would occur within 100 seconds after the initial trigger. Thus, it is hardly surprising that multi-messenger astronomy has only become feasible with modern technology.

In summary, multi-messenger astronomy is a young field of rapid advance. SNe, blazars and GRBs are among the prime candidates for multi-messenger astronomy. In this thesis, I discuss multi-messenger correlations from GRBs, in particular the connection between photons and cosmic rays.

1.2 Gamma-ray bursts

GRBs are the most luminous events in the known universe. They manifest themselves as bright flashes of high-energy electromagnetic radiation, so called gamma-rays, lasting anything from a few tens of milliseconds up to several hours (Mészáros et al., 2019). When a GRB is detected, it outshines its entire host-galaxy, shining brighter than all the other stars combined. During the few seconds that they typically last, they release the

same amount of energy that the sun will have emitted during its entire ten billion year lifetime ($\sim 10^{51}$ erg).

As gamma-rays cannot penetrate Earth's atmosphere, GRBs eluded detection until the advent of space borne satellites. The first GRB was discovered by accident during the cold war by the Vela satellite mission in 1967. The intent of the Vela mission was to monitor the gamma-ray background. This would enable the United States to make sure the Soviet Union did not violate the Partial Test Ban Treaty, which forbade any nuclear detonations above ground. Instead, the Vela satellite discovered emission that did not match any expected signal (Schilling, 2002). When the data was declassified six years later, it promptly resulted in hundreds of theoretical models trying to explain the discovery.

Initially, GRBs were thought to originate from within the Milky Way. This conclusion was largely due to the ludicrous inferred energies required if the events were extragalactic. Due to the observational challenges involved with short duration and atmospheric opacity, the first major break through was not until nearly twenty years later with the launch of the Burst and Transient Source Explorer (BATSE) instrument in 1991. As one of the four main instrument onboard the Compton Gamma-Ray Observatory (CGRO), BATSE was specifically designed to discover GRBs. And discover GRBs it did. During its nine year mission, it detected roughly one GRB per day on average, totaling over 2700 sources. One of the most revealing results of BATSE was the discovery that the distribution of GRBs is isotropic, i.e., they are evenly distributed over the sky. This disfavored them as galactic sources, as one would expect such a population to be focused in the galactic plane. In Figure 1.1, the sky-catalog of BATSE sources can be seen.

Today, it is indeed known that they are from beyond our own galaxy. With the detection of the so called afterglow, lower energy, longer lasting radiation following the prompt emission, their true distances could be determined. Subsequently, their intrinsic energy released could be calculated and it was established that GRBs are the most luminous events in the Universe. More than half a century since their original discovery, many properties of GRBs still remain highly debated.

1.3 Cosmic rays

More than a century ago, Austrian physicist Victor Hess made a series of famous balloon flights. The experiments were based on results found some years prior by German physicist Theodor Wulf. At the time, experimental apparatuses called electroscopes registered a continuous ionizing radiation of unknown source. The leading hypothesis was that the source was terrestrial. To test this hypothesis, Theodor Wulf in 1909 brought an electroscope up

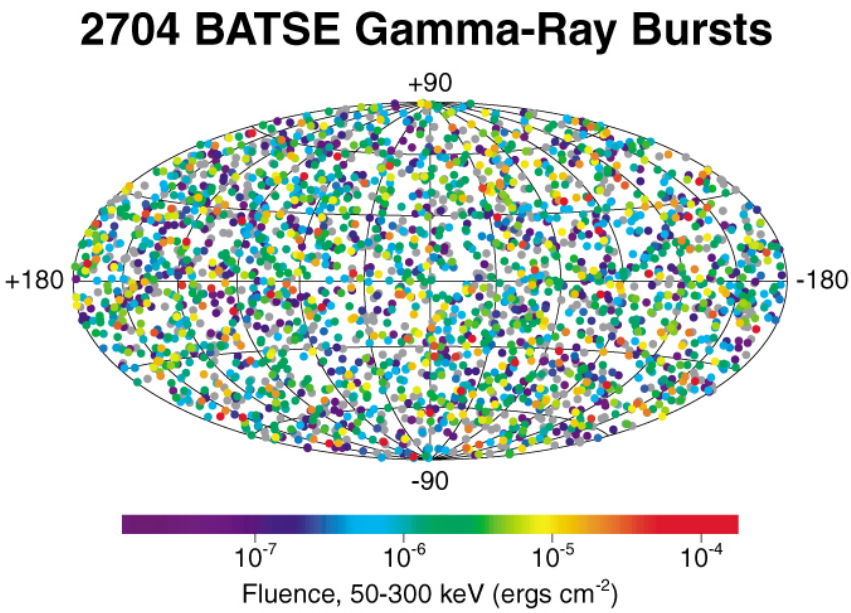

Figure 1.1. BATSE GRB sky-catalog. Each dot is a detected GRB and the color coding gives the GRB fluence (energy per unit area). It is clear that the distribution is isotropic with no specific concentration around the galactic plane. This was a clear indication that GRBs were cosmological events rather than galactic. Figure adopted from NASA Science Official (2019).

to the top of the Eiffel Tower. Surprisingly, the radiation levels did not decrease as predicted (Wulf, 1910). With a similar experimental setup, Victor Hess made a balloon flight in 1911 to an altitude of 1100 m and confirmed Wulf's results. In 1912, Hess ascended to 5300 m during a solar eclipse. The radiation levels still did not decrease. From this he concluded that the source of the radiation was neither the Earth, nor the Sun, but that it was coming from further out in space (Hess, 1912).

The ionizing radiation that Hess had discovered was CRs. CRs are ill-named, as they are not rays at all but energetic particles that are present everywhere in our cosmos. CRs are accelerated to their high energies by various events in the Universe. Some are indeed accelerated in the Sun, some in the outflows of exploding stars, and some in the jets of supermassive black holes in the center of galaxies. The number flux of CRs, that is the number of particles detected per unit area per unit time, extends with a near-perfect power-law over more than ten decades of energy (see Figure 1.2). At low energies, the number flux is dominated by the Sun and the number of particles detected is vast. CRs at intermediate to high energies are mainly accelerated at the shocks of remnants of old SNe. These all have a galactic origin.

At the highest energy end, we have what is known as the ultra-high-energy cosmic rays (UHECRs). These are incredibly rare, with fewer than one particle detected per square kilometer per year. UHECRs have energies extending from a few 10^{18} eV to beyond 10^{20} eV. For comparison, 10^{20} eV is the kinetic energy of a billiard ball traveling at a velocity of 15 m/s. For a UHECR, this energy is contained in one single particle (or nucleus). One of the biggest questions in astrophysicstoday is where UHECR originate from. They are most likely from beyond the Milky Way as our galactic magnetic field is not strong enough to contain them. Because they are so rare, it means that UHECR detectors need to cover vast areas. The biggest detector today is the Pierre Auger Observatory in Argentina, which covers a land area of 3000 km^2 (Abraham et al., 2004). For comparison, Gotland, the biggest island in Sweden, is $\sim$ 3200 km^2. Even with such a tremendous land coverage, the statistics UHECR spectrum is still low. In Paper I and II, we investigate whether GRBs can be the main sources of these eluding particles.

1.4 Context

In a rapidly evolving field, multi-messenger astronomy is becoming more and more important, giving rise to unprecedented sets of data. With the possibility of observing several, different messengers from the same event, it is crucial to know the interplay between them. Specifically, the origin

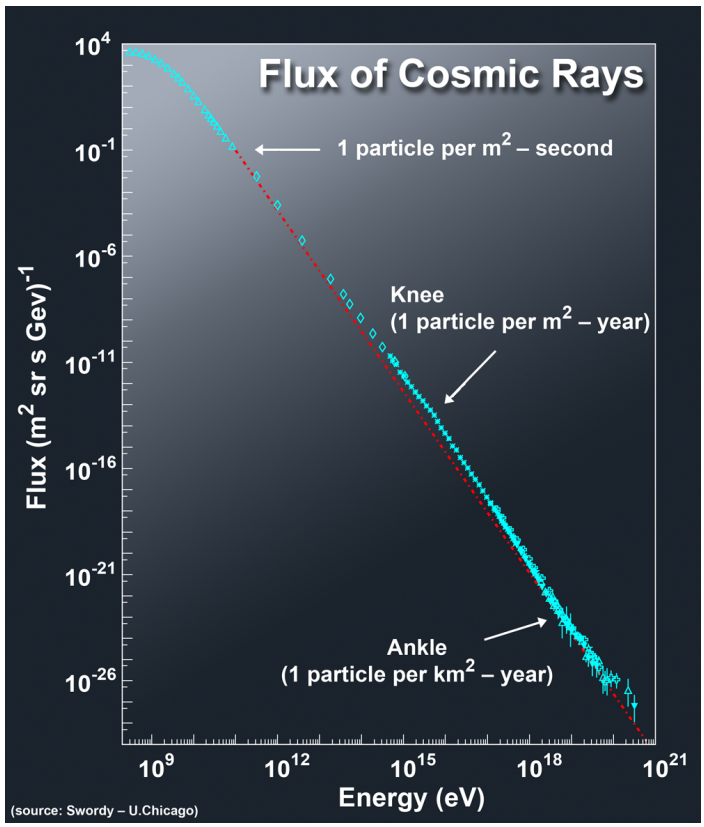

Figure 1.2. The observed CR spectrum. It extends over more than ten orders of magnitude in energy with an almost perfect power-law slope. Only a few signatures can be discerned in the spectrum: the knee at a few 10^{15} eV and the ankle at a few 10^{18} eV. The highest energy CRs are incredibly rare. Figure adopted from Pinfold & Atlas Collaboration (2017).

of UHECR and of the related very-high-energy neutrinos are key questions is astrophysics today. GRBs and UHECRs allows us to study physics in environments too extreme to recreate here on Earth. Thus, they are some of the few laboratories that allow us probe physics on these scales.

In Paper I and II, we study whether GRBs can be the main source of UHECRs. Specifically, we study the connection between the observed radiation spectrum and the acceleration of UHECRs. We make predictions of typical signatures that could be expected if successful UHECR acceleration were to occur. Such signals can be used in future studies. Both Paper I and II give important constraints on GRBs as cosmic ray sources. The methods used in both papers are general and can be applied to many other different sources as well.

1.5 Conventions

In this Section, I mention some of the important physical quantities and nomenclature used in the astronomy community. Hopefully, this may help the unexperienced reader in some of her inevitable confusion when reading this thesis.

This thesis and the astronomy community in general work within the centimeter-gram-second (CGS) unit system, as compared to the standard SI-system. Energies of individual particles are most often given in *electron volts* (eV). The electron volt is defined as the kinetic energy an electron initially at rest gains when accelerated in an electric potential of 1 volt. Some typical energies are the energy of optical photons ~ 1 eV, the proton rest mass energy ~ 1 GeV, and UHECRs > 1 EeV (10^{18} eV). Collective energies of events are given in erg, where 1 erg $= 10^{-7}$ joule. The total energy output of a GRB is 10^{51}–10^{54} erg.

The *luminosity* [erg s^{-1}] of an event is its energy output per unit time. It is common to define different types of luminosities, such as the *radiation luminosity* being the energy output specifically in radiation per unit time. *Flux* [erg s^{-1} cm^{-2}] is energy per unit time per unit area. If the distance d to the object is known, the observed flux F is related to the intrinsic (original) luminosity of an object as L by $F = L/4\pi d^2$. Here, I ignored extinction that occur during the propagation to Earth. The *fluence* [erg cm^{-2}] of an event is the flux integrated over the event duration (see Figure 1.1). For radiation, the *spectral flux density* [erg s^{-1} cm^{-2} Hz^{-1}] is the flux per unit frequency. The spectral flux density denoted by F_ν is sometimes called the specific flux, spectral flux, or simply flux. As the frequency of a photon is directly proportional to its energy, the spectral flux density can also be given by F_ε [erg s^{-1} cm^{-2} eV^{-1}]. In radio astronomy, it is common to use to unit Jansky (Jy), defined as 1 Jy$= 10^{-23}$ erg s^{-1} cm^{-2} Hz^{-1}.

Detected signals contain information about the arrival time of particles and their energies. A figure that plots particle number (or flux) versus arrival time is called a *light curve*. A light curve can be shown for particles within a specific energy range. A *spectrum* plots differential particle number (or differential flux) versus energy. A spectrum requires a specified time interval to indicate what particles are included. A *time integrated* spectrum includes all particles observed from an event while a *time resolved* spectrum shows only particles within a specific time range.

The prefix *circum* is often used to mean "around". For instance, circumstellar material means the material surrounding a star. For GRBs, the circumburst medium is the medium surrounding the GRB explosion. Similarly, *inter* is used to describe "in between". The intergalactic medium is the material between galaxies.

In astrophysics, one often has to account for the effects of special relativity, which implies that quantities are measured differently by different observers. Therefore, it is necessary to define in which frame a quantity is measured. Quantities measured in frames that are moving relative to a stationary lab frame on Earth is often denoted by primes. In a relativistic jet, the time measured by an observer moving with the jet would be denoted t' while the time measured by a stationary observer on Earth would be denoted t.

Another consequence of relativity is *redshift*. When looking out into space, one is also looking back in time. The speed of light is not infinite and it takes time for the light to propagate from its origin to us. Signals that we observe today can can have been created hundreds of million years ago and very distant objects observed where created in a time when the Universe was younger. As the universe is expanding, waves of a original wave length gets "stretched out". As light with longer wavelength is less energetic, this is known as *cosmological redshift* as it shifts light to lower-energy, redder light. Due to particle-wave duality of quantum mechanics, this energy shift also affects particles. The redshift of an object is denoted by z and an observed energy $E_{\rm obs}$ is related to an original energy E_{source} as $E_{\rm obs} = E_{\rm source}/(1+z)$. More distant object have larger redshift with Earth being at $z = 0$.

Sometimes, spectra are described as *hard* or *soft*. A hard spectrum has a high *hardness ratio*, which is defined as the ratio of observed particles with higher energy to observed particles with lower energy. Here, higher and lower energy are arbitrary energy bands and thus there exists several different hardness ratios. It is useful to speak of a hard/soft spectrum as different acceleration or radiation mechanisms naturally produces different ratios of high- to low-energy particles.

Lastly, one often uses the shorthand notation $Q_X \equiv Q/10^X$ for quantities Q. This is very useful to get an estimate of the magnitude of a quantity while still seeing its parameter dependence. For example, in GRBs, the emission radius r can be estimated from the observed variability time t and Lorentz factor of the outflow Γ as $r = 2ct\Gamma^2$, where $c = 3 \times 10^{10}$ cm s^{-1} is the speed of light in vacuum. Typical values are $t \sim 1$ s and $\Gamma \sim 100$ so one can write $r = 6 \times 10^{14}\ t_0\ \Gamma_2^2$ cm. If one observes a GRB with a variability time of only $t = 50$ ms, it is then easy to estimate from this expression the emission radius as $r = 3 \times 10^{13}$ cm.

Chapter 2

Physical processes

In this chapter, I will outline some of the basic physics needed to understand subsequent chapters. This will in no way be a complete account of the different mechanisms at hand but a general overview. For more detailed descriptions, I refer to designated text books on each subject.

2.1 Relativity

In a landmark paper published in 1905, Einstein laid out the framework of special relativity (Einstein, 1905b). In the paper, he makes two postulates: 1) There is no such thing as an absolute rest frame, physical laws remain identical regardless of the apparent speed of the coordinate system in which they are observed and 2) the speed of light in vacuum c is constant and identical for all observers, even if that observer has a relative velocity to the source of the light. Given these two deceptively simple postulates, it follows that neither time nor space are absolute but depend on the relative motion between observers (Einstein, 1905b).

When things move with velocities close to the speed of light, one refers to them as *relativistic*, because one must account for the effects of special relativity. GRBs outflows are accelerated to such a degree that they become highly relativistic. The electrons in the outflow, responsible for the radiation that we observe are also relativistic. The vast energies of UHECR makes them extremely relativistic particles. Unfortunately, there is no way of giving a full description of special relativity here. It is furthermore one of the most confusing concepts in all of physics. For a good introduction, I refer to chapter 2 of Harris (2008). Here, I only give a short account of the relevant effects.

Time dilation

An example of how Einstein's two simple postulates can have such profound consequences is as follows. Imagine two people standing on a train that is moving with a velocity v in a straight line. They are standing a distance l away from each other. A second pair of people are standing slightly further apart ($l + \Delta l$) by the side of the train tracks. The person in the back of the train is holding a flash light aimed at the second person on the train. At the exact moment when the person with the flash light passes the first person by the train tracks, she turns the flash light on. The experiment is set up such that the light reaches the second person on the train exactly when she passes the second person by the train tracks. By postulate 1), there is no difference to the physics on a moving train. Thus, for the pair of people on the train the distance traveled by the light is simply l. However, for the pair of observers by the train tracks the distance is slightly longer, since the train has had some time to move during the light travel time. By postulate 2), both pairs see the light moving with a fixed velocity c (3×10^{10} cm s^{-1}), so how can this be? The solution is that time is not absolute. For the observers outside, the distance traveled by the light is slightly larger. Therefore, more time must have elapsed for them as compared to the observers on the train, the time on the train moves slower. The phenomenon that time slows down on a moving clocks as compared to a stationary clock is called *time dilation*.

Lorentz factor. The Lorentz factor γ (pronounced *gamma*) is a central concept of relativity. The Lorentz factor γ (or Γ) is only a function of the velocity and is defined as

$$\gamma = 1/\sqrt{1 - (v/c)^2}. \tag{2.1}$$

As $0 \leq v < c$, it is always true that $\gamma \geq 1$. When γ starts to grow larger than 1, traditional Newtonian mechanics breaks down. All object around us has an associated Lorentz factor. However, the speed of everyday objects are always so far from the speed of light that the effects of relativity are unnoticeable. In astrophysics, this is no longer the case. In GRB physics, one often refers to bulk Lorentz factor of the outflow by capital Γ and the Lorentz factors of particles (electrons, protons and nuclei) by lower case γ'. Here, the prime denotes that the Lorentz factor is most often evaluated in the outflow frame, i.e., the particles are relativistic even as seen from an observer traveling with the outflow.

Time dilation and length contraction. Imagine a relativistic outflow with Lorentz factor Γ. The time t' as measure in the outflow frame between two

events occurring at the same place in the outflow frame, will be separated by a longer time t for the observer on Earth (time is dilated). The relation between t' and t is given by

$$t = \gamma t'. \tag{2.2}$$

The length l' of an object at rest in one frame will be contracted for an observer that is moving relative to this frame by

$$l = \frac{l'}{\gamma}. \tag{2.3}$$

Beaming. Driving a car while the rain is pouring down, it is possible to get the sensation that the rain drops are hitting the wind shield almost vertically, although the rain is falling straight towards the ground. A related effect happens with moving emitters of light. Radiation emitted isotropically by a source moving with a velocity v compared to an observer on Earth, will be beamed in the direction the source is moving. The beaming will be such that half of the emitted radiation will be beamed into a cone with opening angle $\theta \sim 1/\gamma$, where γ is the Lorentz factor of the emitter. A consequence is that objects moving away from us with $\gamma \gg 1$ can be virtually undetectable, as most of the light is beamed in the opposite direction.

Blueshift, redshift and Doppler factor. Radiation emitted with a frequency ν_{source} by a moving source will be observed as having a different frequency ν_{obs}. The two frequencies are related as

$$\nu_{\text{obs}} = \delta\nu_{\text{source}} = \gamma\nu_{\text{source}}\left(1 + \frac{v}{c}\cos\theta\right), \tag{2.4}$$

where v is the velocity of the emitter and θ is the angle between the velocity vector of the source to the line of sight. The factor $\delta \equiv \gamma\left(1 + \frac{v}{c}\cos\theta\right)$ is called the relativistic Doppler factor. The parenthesis accounts for the traditional Doppler shift that one hears when an ambulance drives by. The γ-factor is a relativistic effect that accounts for time dilation, which makes the time between subsequent pulses in the source frame longer.

An observed photon is blueshifted if the observed frequency is higher than the emitted frequency (source moving towards the observer) and redshifted otherwise. The names stem from the fact that blue, visible light is more energetic than red light. However, the terms blue- and redshift is used for all electromagnetic bands, not just in the optical.

2.2 Astrophysical messengers

The Universe is not a vacuum. Granted, the density of particles is roughly 10^{19} times less than air but particles still exists all around. Every particle

carries with it information, such as its energy and direction. The collective detection of many particles can tell a comprehensive story. For instance, when a SN explodes it releases an unimaginable number of neutrinos and photons.

Simply put, an astrophysical messenger is something that brings us information regarding the Universe, a message from space. In this sense, every particle that we detect is a messenger, i.e., carries information. One often differentiates between different types of messengers. In multi-messenger astronomy there exists four different types, which I explain in more detail below.

2.2.1 Photons

Photons, the quanta of electromagnetic (EM) radiation, has historically been our only way of gaining information regarding the Universe. It is still beyond a doubt the most important. There are various different names for EM radiation but it is all part of the same phenomenon and solely depends on the energy. From lower to higher radiation energy, EM radiation includes: radio, infrared, optical, ultraviolet, X-rays, and gamma-rays.

All EM radiation travel with the speed of light. Because of the particle-wave duality of quantum mechanics, EM radiation is both a wave, with an associated wavelength and frequency, and discrete particles (photons). At lower energies the wave description is most tractable and radio astronomers study radio waves. At higher energies, each quanta has enough energy to be separately detected, so X-ray and γ-ray astronomers work with photons. As the radiation travels at c in vacuum, the wavelength λ and frequency ν is related by $\lambda = c/\nu$. The frequency ν of a photon is still used for X-ray and γ-ray astronomy and the associated energy of the photon is $\varepsilon = h\nu$, where h is Planck's constant.

2.2.2 Cosmic rays

CRs introduced in Section 1.3, is one of the four messenger types. Unfortunately, it is difficult to use them for scientific research as they are charged. Charged particles are deflected in magnetic fields. The galactic magnetic field of the Milky Way bends the trajectories of CRs. Therefore, they do not point back to their source of origin. Despite this, they are interesting in their own right. Specifically, the UHECRs can tell us about particle physics at energies that are impossible to recreate in any laboratory on Earth.

Experiments designed to detect UHECR do not detect the particles directly. When an UHECR enters the atmosphere, it interacts with the dense

surrounding. The interactions create secondary particles such as pions, neutrinos, and gamma-rays. The large energy of the incoming particle gets imparted into the secondaries. Thus, these are themselves energetic enough to create further particles by e.g., by pair production. Through various reaction a shower of particles is created an *extensive air shower*. It is the extensive air showers that the experiments detect.

One of the detections methods used are water Cherenkov detectors. This method is used in for instance the Pierre Auger experiment mentioned in Section 1.3. Water Cherenkov detectors are large water tanks spread out across the detector area. Each water tank is surrounded by sensitive photomultiplier tubes that can detect light. When the extensive air shower reaches the ground, many of the particles are highly relativistic and these can travel faster than the speed of light in the water (which is lower than c). Through a phenomenon similar to that of breaking the sound barrier, charged particles moving quicker than the speed of light in a material creates in its wake a cone of light called Cherenkov radiation. The photomultiplier tubes in the water Cherenkov detectors are able to detect this radiation. Depending on the amount of light received and in which sequence the water tanks receive the signal, information regarding the original UHECRs energy and direction can be obtained.

2.2.3 Neutrinos

Neutrinos are elementary particles present in enormous abundances all throughout space. Neutrinos only interact through the weak force and are therefore notoriously difficult to detect. During the neutrino burst of SN 1987A, the Kamiokande experiment that was the biggest neutrino detector at the time, manage to detect twelve neutrinos out of the 10^{16} that passed through the detector (Nobel Media AB, 2002). However, this small number was enough to grant them part of the 2002 Nobel Prize in Physics.

Most neutrino detectors look for Cherenkov radiation emitted by the secondaries to a neutrino interaction, similarly to UHECR detectors. However, when a high-energy neutrino interacts in a material it imparts some of its energy to a single charged secondary particle, i.e., no showers are created. Because neutrinos interact so incredibly seldom the experiments that wish to detect them need to cover large volumes. Furthermore, as they are looking for radiation the material in which the neutrino interacts cannot be opaque. The biggest neutrino experiment today is the IceCube observatory located on the South Pole. Using the clear ice as the interaction volume, 86 strings with 60 photo sensors each, so called digital optical modules (DOMs), are evenly spaced in the ice. The neutrino interaction volume that they are sensitive to is a km^3, hence the name.

The astrophysical neutrino energies that IceCube are sensitive to are quite high (~ 10–10^3 TeV). At lower energies, the detections are dominated by atmospheric background. In 2013, the IceCube collaboration revealed they had detected an extraterrestrial diffuse neutrino flux (IceCube Collaboration, 2013). It is still unknown what events are mainly responsible for creating these neutrinos.

The low interaction probability of neutrinos makes them good tracers of their birth site, however pinpointing the sources of individual neutrinos have proven to be very difficult. So far, two detection claims in spatial coincidence with flaring blazars have been made IceCube Collaboration et al. (2018b,a); IceCube Collaboration (2020), however if this constitutes a firm association is not clear (e.g., Keivani et al., 2018). High-energy neutrinos are interesting, as they are bi-products of photohadronic interaction between radiation and high-energy CRs. The photohadronic interaction creates charged pions, which subsequently decay into neutrinos. The energy of the resulting neutrino is roughly 5% that of the parent CR (Hümmer et al., 2010). As such, neutrinos can give us information about CR production in a source. An association of a very-high-energy neutrino with energy 10^{16}–10^{18} eV would be a clear indication of UHECRs at the source. Another bi-product of the photohadronic interaction is gamma-rays through the decay of neutral pions. Many multi-messenger studies of UHECRs tries to simultaneously predict the emitted UHECR and neutrino signal (e.g., Baerwald et al., 2013; Biehl et al., 2017; Boncioli et al., 2019; Heinze et al., 2019), sometimes together with the gamma-ray signal as well (e.g., Murase et al., 2008; Bustamante et al., 2017).

2.2.4 Gravitational waves

Gravitational waves (GWs) are a prediction of general relativity (Einstein, 1915). Gravity bends spacetime. If the gravitational potential of an object is large enough and it moves fast enough, its effect on spacetime is measurable.

Short GRBs (see Section 4.1.2) are created in the mergers of two inspiralling neutron stars. Neutron stars are incredibly dense object and they create deep gravitational potential wells. When the neutron stars circle each other they emit GWs. In the final moments before merger, the two neutron stars travel with a significant fraction the speed of light. The very famous event of GW 170817 mentioned in the Introduction was gravitational waves and a short GRB detected from the merger of two neutron star.

In 2015, the first ever detection of GWs was made (Abbott et al., 2016). This signal was not of two merging neutron stars but of two inspiralling black holes. The observation of gravitational waves was awarded the 2017 Nobel Prize in physics (Nobel Media AB, 2017).

2.3 Radiation processes

Accelerating electric charges emit radiation and this occurs everywhere in the Universe. Some of the most important astrophysical radiation processes are line emission, bremsstrahlung, synchrotron radiation, thermal emission, and inverse Compton scattering. In this Section, I give short descriptions on these different emission mechanisms. The most import radiation process for this thesis is synchrotron emission and it will therefore be explained in more detail in Section 2.5. All processes are described in detail in Rybicki & Lightman (1979).

Line emission. According to quantum mechanics, an atom or molecule can only occupy specific, discrete energy levels. When an atom transitions from one energy level to another energy must be conserved. If the new energy level is lower than the original one, a photon is emitted carrying an energy equal to the energy difference between the two levels. Photons emitted this way therefore have characteristic energies depending on which transition has occurred. From the photon energy, the specific parent atom and transition can be deduced. Such emission is called line emission due to the spike it creates in a spectrum, resembling a single line around the characteristic energy with no emission at other energies.

Line emission is extremely useful in astrophysical studies. Line emission from various atoms and molecules can be studied in controlled lab environments on Earth. An astrophysical spectrum with line emission can then give information depending on how much it deviates from the controlled, Earth spectrum. For instance, an observed spectrum might contain line emission from hydrogen, helium, oxygen, and silicon. However, these lines all seem to fall at slightly lower energies compared to the lab spectrum. The shift can then inform us of the *redshift* of the event, i.e., at what distance from us it occurred. Another example is the broadening of lines, which can tell us about the temperature of sources. Higher temperature implies more random, thermal motion of atoms and molecules within the emitting region. Due to this motion, some emitted photons are slightly redshifted while some are slightly blueshifted. The observed line emission is a superposition of all these photons, which create a broadening of the line. Broader line means higher temperatures of the emitting region. Line broadening also occurs in accretion discs, when one part of the disk moves towards us (blueshifted emission) and one part of the disk moves away from us (redshifted emission). More straight-forward applications of line emission is that it can tell us about the chemical abundances of an event.

Bremsstrahlung. Bremsstrahlung is German and means braking radiation. If free electrons and ions are present in a plasma, their opposite charges cause an attractive force between the two species. A freely stream-

ing electron passing close to a positively charged ion will feel this attraction. This causes a curve in the electron's trajectory. The change of the momentum of the electron results in the emission of radiation that is called bremsstrahlung. The total power of the radiation emitted this way depends on the density of electrons and ions in the emitting region. As a rule, bremsstrahlung is only important in astrophysical scenarios where the particle densities are high and it can quite often be safely ignored. However, bremsstrahlung can be a very important photon generation mechanism, even if those photons do not escape the system and are therefore not directly observable.

Synchrotron radiation. Electric charges in magnetic fields will gyrate around the magnetic field lines. If the charge had some initial velocity parallel to the magnetic field line, this velocity is unaltered. Thus, the charged particles traces out a helical path following the magnetic field line. The gyration means that the particle experiences continuous acceleration and it therefore emits radiation. The frequency of the radiation produced this way is proportional to the gyration period of the charged particle. This type of radiation is called cyclotron radiation. If the particle is relativistic, the emitted radiation is beamed and can only be seen in short, intermittent pulses when the particle is traveling towards the observer. The relativistic case is called synchrotron emission and much more important in astrophysical environments than cyclotron emission. As the observed frequency is inversely proportional to the pulse width according to Fourier analysis, the observed synchrotron frequency is much higher than in the cyclotron case.

Compton Scattering. Existing electrons and photons can interact with each other if they come sufficiently close. This interaction is called scattering and it changes both the directions and energies of the two scatterers. In the case where the incoming photon is more energetic than the incoming electron the photon can impart some of its energy to the electron. This interaction is called Compton scattering. Inverse Compton scattering is where the photon gains energy from the electron. The energy gained by the photon this way is proportional to the Lorentz factor of the electron squared (γ^2). Thus, this process can results in very-high-energy photons. If the scattering between the electron and the photon is elastic, i.e., that no energy is transferred between the two, it called *Thomson scattering*. Thomson scattering is the low-energy limit of Compton scattering.

Inverse Compton scattering is not an emission process in the sense that photons are not produced. However, one often speaks about inverse Compton scattering as an emission process due to the great impact it can have on the observed spectrum.

Thermal radiation. Thermal radiation is the name of the spectrum emitted by matter that is in thermal equilibrium. If this radiation itself has had

time to come into thermal equilibrium before it escapes, it is called blackbody radiation. A blackbody spectrum is described by the Planck function and is only a function of the temperature. It is a theoretical concept that can never truly be reached in nature. Even so, one describes observed spectra as blackbody emission if it resembles a blackbody. For instance, the sun is an almost perfect blackbody. Similarly to Compton scattering, thermal emission does not produce any photons. Indeed, thermal radiation does not specify how the photons are created. Any emission process, e.g., bremsstrahlung, results in an emitted blackbody spectrum as long as the radiation has had time to come into thermal equilibrium.

In a GRB jet, the outflow is a plasma consisting of charged particles (leptons and baryons), radiation and magnetic fields. The charged particles interact with the photons exchanging energy between one another. This interplay eventually lead to thermodynamical equilibrium between all species. However, in the outflow the ratio of photons to charged particles is very high ($\sim 10^5$). During the typical time it takes a photon to interact once, the charged particles have undergone 10^5 interactions. Thus, the charged particles thermalize much quicker than the photons, hence it is not necessarily true that the radiation is in thermal equilibrium even though the particles are. Whether or not radiation has time to come into thermal equilibrium depends on the optical depth at which it is generated (see Section 2.4).

2.4 Absorption processes and optical depth

All emission processes comes with an associated absorption process. For instance, if an atom or molecule interact with a photon of characteristic energy, it can transitions from a lower energy state into a higher by absorbing the photon. This is equivalent but opposite to line emission and is called *line absorption*. If the photon is more energetic than the binding energy of an electron in an atom, the electron can become unbound. This phenomenon is known as photoelectric absorption (photoelectric effect), the study of which lead Einstein to suggest the existence of photons and to him receiving the Nobel Prize in Physics 1921 (Einstein, 1905a). Synchrotron self-absorption is the process where the charged particles responsible for the synchrotron emission themselves partially reabsorb the emission. This occurs at low photon energies and will lead to a sharp decline in observed emission below the a specific self-absorption frequency.

Of specific interest in this thesis is the concept of *optical depth*. The optical depth τ is a measure of how likely a photon is to be absorbed while

moving between r_0 and r. It is defined as

$$\tau(r) = \int_{r_0}^{r} n(\tilde{r})\,\sigma(\tilde{r})\,d\tilde{r}, \tag{2.5}$$

where $\tilde{r}$ is a parameter of integration and n is the particle density that can vary along $\tilde{r}$. The parameter σ is called the *cross section*.

Cross section

Imagine a slab of width dx [cm]. Inside the slab, there are lots of particles distributed with a number density n [cm^{-3}]. What is the probability P that a photon traveling towards the slab gets absorbed within the slab? Obviously, it is a function of the particles density n. It is also a function of the width dx, the wider the slab, the higher the probability of absorption. Lastly, it is a function of the cross section σ [cm^2] such that $P = \sigma n dx$. The intuitive way to think about the cross section is the influential area surrounding each of the particles in the slab. If the photon passes within this area, it is close enough to the particle to be absorbed.

In Equation (2.5), the absorption process is not specified. It is possible to look at the optical depth of a specific absorption process by inserting the cross section for that particular absorption (see e.g., Rees & Mészáros, 2005). However, it is often of interest to see only whether a photon will be absorbed or not. It is also common to include scattering in the expression the cross section, in which case the optical depth becomes a measure of how likely a photon is to interact. Scattering is an absorption process in the sense that it can change the direction and energy of the photon (so in a beam of radiation with specified energy and direction it can be considered lost) however the photon is not destroyed. A medium is said to be *optically thick* if the optical depth integrated over the medium size is larger than unity: $\tau > 1$. Else, the medium is *optically thin*. The photospheric radius of a GRB (see Section 4.2.2) is defined as the radius where the optical depth of the GRB jet drops below one. Beyond the photospheric radius, the jet is optically thin and photons can stream freely and reach the observer without further interaction.

2.5 Synchrotron radiation

Synchrotron radiation is an important radiation mechanism in astrophysics and specifically in GRB physics. For one, it is most certainly responsible for the afterglow emission that is explained in Section 4.3. Additionally, several

prompt models predict the observed prompt radiation is due to synchrotron. Synchrotron emission is important in this thesis because acceleration of UHECR requires strong magnetic fields. As briefly explained in Section 2.3, relativistic electrons in magnetic fields emit synchrotron radiation. In Paper I and Paper II, we exploit this fact by characterizing the inevitable synchrotron radiation emitted by electrons that are co-accelerated at the UHECR acceleration site. We compare this estimated radiation to GRB observations to see whether GRBs are compatible with UHECR acceleration or not.

In this section, I describe theoretical aspects of synchrotron radiation in more detail. These concepts are important for the methodology in Paper I and II. To be consistent with the papers and this thesis, I work under the GRB framework of synchrotron radiation. As such, I denote physical quantities by primes to indicate that they are evaluated in the frame comoving with the relativistic outflow. Unprimed quantities is evaluated in the observer frame. However, note that the primed quantities are the predictions from synchrotron theory, which are equally valid in a stationary picture. It is the unprimed quantities that have been transformed.

2.5.1 Characteristic timescale

The total synchrotron power P' averaged over pitch angle emitted by one charged particle with Lorentz factor γ', mass m, and charge number Z in a magnetic field B' is given by (e.g., Rybicki & Lightman, 1979)

$$P' = \frac{4}{3}\sigma_{\rm T} Z^4 \left(\frac{m_e}{m}\right)^2 c\beta'^2\gamma'^2\frac{B'^2}{8\pi}. \tag{2.6}$$

In the equation above $\sigma_{\rm T}$ is the electron Thomson cross section and β' is the velocity of the charged particle in terms of speed of light c. From Equation 2.6 it is evident that the power emitted is inversely proportional to the mass of the emitter squared. Therefore, it is most commonly assumed that electrons are the particles dominating the observed radiation, rather than protons or other heavier charged particles. However, I note that alternative theories exists (Ghisellini et al., 2020).

The power is energy emitted per unit time. In the differential limit, we have $P' = -dE'/dt'$, where $E' = \gamma' mc^2$ is the energy of the particle, t' is the time, and the minus sign appears because the particle is losing energy. Inserting this into Equation (2.6), assuming the particle is highly relativistic $\beta' \sim 1$, and separating variables one gets

$$-\frac{dE'}{E'^2} = \frac{4}{3}\sigma_{\rm T} Z^4 \left(\frac{m_e}{m}\right)^2 \frac{c}{(mc^2)^2}\frac{B'^2}{8\pi}dt'. \tag{2.7}$$

Integrating both sides and assuming the magnetic field stays constant under the time scale considered implies

$$\begin{aligned} -\int_{E'_{\rm initial}}^{E'_{\rm final}} \frac{d\tilde{E}'}{\tilde{E}'^2} &= \frac{1}{E'_{\rm final}} - \frac{1}{E'_{\rm initial}} \\ &= \frac{4}{3}\sigma_{\rm T} Z^4 \left(\frac{m}{m_e}\right)^2 \frac{c}{(mc^2)^2}\frac{B'^2}{8\pi}(t'_{\rm final} - t'_{\rm initial}). \end{aligned} \tag{2.8}$$

The time it takes the particle to lose half of its energy due to synchrotron radiation is thus

$$t'_{\rm sync} = \frac{6\pi}{Z^4\sigma_{\rm T}}\left(\frac{m_e}{m}\right)^2 \frac{(mc^2)^2}{c}\frac{1}{E'B'^2}, \tag{2.9}$$

where we have simply called $E'_{\rm initial}$ for E'. The timescale $t'_{\rm sync}$ is called the *synchrotron energy loss timescale*, or the *characteristic synchrotron timescale*, for a particle of energy E'. It gives an estimate of how long time it takes for a particle in a magnetic field with strength B to lose a significant fraction of its energy to synchrotron radiation.

2.5.2 Characteristic frequency

The angular frequency ω' in the non-relativistic case can be obtained by equating the centripetal force to the Lorentz force:

$$ma'_{\rm centripetal} = \frac{q}{c}(\mathbf{v}'_\perp \times \mathbf{B}'), \tag{2.10}$$

where $\mathbf{v}'_\perp$ is the component of the velocity that is perpendicular to the magnetic field B'. The magnitude of the centripetal acceleration is $a'_{\rm centripetal} = v'/r'^2$. Solving for the angular velocity $\omega' \equiv v'/r'$, one gets

$$\omega'_{\rm NR} = \frac{qB'}{mc}. \tag{2.11}$$

The frequency in equation (2.11) is called the *cyclotron frequency* (subscript NR stands for non-relativistic, true in the outflow frame). The rotational frequency ν' is equal to $\nu' = \omega'/2\pi$. In the relativistic case, the emitted radiation is boosted by a factor of γ'^2. The observed spectrum from an electron with Lorentz factor γ' will cover a range of energies but the *characteristic synchrotron frequency* emitted is

$$\nu' = \frac{qB'}{2\pi mc}\gamma'^2. \tag{2.12}$$

2.5.3 Photon spectrum

From Equation (2.12) it is evident that the observed spectrum depends on the Lorentz factors of the emitters and hence on electron distribution. In this Section I first define three important electron Lorentz factors and then I explain how they affect the spectrum.

In GRB applications, the shape of the spectrum is characterized by three specific electron Lorentz factors: the injection Lorentz factor $\gamma'_{\rm m}$, the cooling Lorentz factor $\gamma'_{\rm c}$ and the self-absorption Lorentz factor $\gamma'_{\rm SSA}$. Below I explain the meaning of these three in turn.

Injection Lorentz factor. In GRBs and other astrophysical sources, one often assumes that the source distribution of electrons is a power-law. This is consistent with the theory of diffusive shock acceleration described in Section 3.1. A power-law in energy means that the number of electrons at higher energies decreases as the energy to some power. If the total number of accelerated electrons is N, this is written as

$$\frac{dN}{d\gamma'} = C'\gamma'^{-p}, \qquad \gamma'_{\rm m} < \gamma' < \gamma'_{\rm max} \tag{2.13}$$

where C' is some proportionality constant and the power-law extends from the minimum Lorentz factor $\gamma'_{\rm m}$ to the maximum Lorentz factor $\gamma'_{\rm max}$. The variable p is called the *electron spectral index*. It determines the slope of the power-law spectrum. If p is small, the spectrum is said to be hard. If p is large, the spectrum is soft and fewer particles exists at higher energies. It can be useful to note that if $p = 1$, the number of particles per decade energy is the same, while if $p = 2$ the energy carried by the particles per decade energy is the same. I will assume $p > 2$ in the following derivation.

The minimum Lorentz factor $\gamma'_{\rm m}$ is ofter called the *injection Lorentz factor*. The name comes from the picture that electrons passing a shock are injected into the acceleration process. Hence, the electrons that immediately exit the acceleration process only have the injection energy equal to $\gamma'_{\rm m}mc^2$. The value of $\gamma'_{\rm m}$ is important as it determines the shape of the spectrum. I will presently give a rough derivation of its value following e.g. Mészáros (2006). From equation (2.13) the number of electrons in the power law can be obtained

$$N = \int_{\gamma'_{\rm m}}^{\gamma'_{\rm max}} C'\tilde{\gamma}'^{-p} d\tilde{\gamma}' = \frac{C'}{p-1}\left(\frac{1}{\gamma'^{p-1}_{\rm m}} - \frac{1}{\gamma'^{p-1}_{\rm max}}\right). \tag{2.14}$$

The energy in the accelerated electrons is

$$E'_e = C'm_ec^2 \int_{\gamma'_{\rm m}}^{\gamma'_{\rm max}} \tilde{\gamma}'^{-p+1} d\tilde{\gamma}' = \frac{C'm_ec^2}{p-2}\left(\frac{1}{\gamma'^{p-2}_{\rm m}} - \frac{1}{\gamma'^{p-2}_{\rm max}}\right). \tag{2.15}$$

Solving for C' from equation (2.14), we obtain

$$C' = N(p-1)\left(\frac{1}{\gamma_{\rm m}'^{p-1}} - \frac{1}{\gamma_{\rm max}'^{p-1}}\right)^{-1}. \tag{2.16}$$

Inserting into equation (2.15) yields

$$E_e' = N m_e c^2 \gamma_{\rm m}' \frac{(p-1)}{(p-2)} \left(\frac{1-\left(\frac{\gamma_{\rm m}'}{\gamma_{\rm max}'}\right)^{p-2}}{1-\left(\frac{\gamma_{\rm m}'}{\gamma_{\rm max}'}\right)^{p-1}}\right) \tag{2.17}$$

It is often assumed that $\gamma_{\rm max}' \gg \gamma_{\rm m}'$. With this assumption, together with $p > 2$, the large parenthesis in Equation (2.17) is simply 1.

To proceed, one introduces the dimensionless quantity ϵ_e. It is defined as the fraction of the internal energy behind the shock that is given to the accelerated electrons. In a shock scenario, the shock will dissipate some of the kinetic energy and turn it into internal energy $E_{\rm int}'$. Let's assume the material in front of the shocks is stationary and consisting of protons and electrons. In the rest frame of the shock, the incoming particles will have a kinetic energy $N_p(\Gamma-1)m_pc^2 + N_e(\Gamma-1)m_ec^2 \approx N_p(\Gamma-1)m_pc^2$, where Γ is the shock Lorentz factor and N_p and N_e are the number of protons and electrons respectively. This is the energy that is converted into internal energy behind the shock. Out of this available energy, the accelerated electrons will get some fraction ϵ_e, i.e., $E_e' = \epsilon_e N_p(\Gamma-1)m_pc^2$.

The last thing to do is introduce the fraction ξ_a as the number fraction of electrons that are accelerated into the power-law out of the total bulk number. Assuming that there is charge neutrality, then $N_e = N_p$. Thus, one gets $N = \xi_a N_e = \xi_a N_p$. Putting this all together, one can solve foe $\gamma_{\rm m}$ in Equation 2.17 as

$$\gamma_{\rm m}' = \frac{p-2}{p-1}(\Gamma-1)\frac{m_p}{m_e}\frac{\epsilon_e}{\xi_a}. \tag{2.18}$$

The dependence of $\gamma_{\rm m} \propto \epsilon_e/\xi_a$ is quite intuitive. The more energy given to the accelerated electrons (larger ϵ_e), the higher the $\gamma_{\rm m}$ and the fewer electrons share this energy (smaller ξ_a) the higher the $\gamma_{\rm m}$.

Cooling Lorentz factor. The electrons in the outflow mainly lose their energy in two different ways, through their synchrotron emission and through the adiabatic expansion of the jet. The time scale for synchrotron energy losses has already been described in Section 2.5.1. The adiabatic losses come from the fact that as the jet moves outwards, it expands. The expansion implies that the internal particles do work on the system. Macroscopically, it is a similar effect as when the temperature drops in a gas that expands in accordance to the ideal gas. Microscopically, the effect occurs because in

an expanding medium, the electrons are statistically more likely to interact with particles moving away from them than towards them, leading to an average energy loss.

For a reversible, adiabatic process, the temperature T is related to the volume V as $T \propto V^{1-\gamma_{\rm ad}}$, where $\gamma_{\rm ad}$ is the adiabatic index (not to be confused with a Lorentz factor). As the GRB outflow is radiation dominated, the adiabatic index is $\gamma_{\rm ad} = 4/3$. The comoving volume is proportional to the radius cubed, which indicates that the comoving temperature drops as $T' \propto r^{-1}$. As the internal energy of the particles is proportional to the temperature, it follows that a particle loses half of its energy due to the adiabatic expansion of the jet when $r \to 2r$. The corresponding timescale is

$$t'_{\rm ad} = \frac{r}{2c\Gamma}, \tag{2.19}$$

where the factor of Γ enter due to the length contraction of r in the outflow frame. In the literature, the factor of $1/2$ is often dropped.

The *cooling Lorentz factor* of the electrons $\gamma'_{\rm c}$ is defined as the Lorentz factor where an electron would lose equal amount of energy to synchrotron radiation as to the adiabatic expansion of the ejecta. It can be obtained by equating equations (2.9) and (2.19) (where the factor of $1/2$ in Equation (2.19) has been dropped)

$$\gamma'_c = \frac{6\pi m_e c^2}{\sigma_{\rm T}} \frac{\Gamma}{rB'^2}. \tag{2.20}$$

As $t'_{\rm ad}$ is independent of energy while $t'_{\rm sync} \propto \gamma'^{-1}$, electrons with Lorentz factor $\gamma' > \gamma'_{\rm c}$ cool mainly through synchrotron emission while electrons with Lorentz factor $\gamma' < \gamma'_{\rm c}$ cool mostly due to the adiabatic expansion.

Self-absorption Lorentz factor. The last important Lorentz factor is $\gamma'_{\rm SSA}$. The electrons that emit synchrotron radiation can themselves absorb the same radiation through synchrotron self-absorption. The absorption is preferential to low-energy emission leading to a sharp drop of the spectrum at low energies. Electrons with Lorentz factors less than $\gamma'_{\rm SSA}$ effectively reabsorb photon, which increases their energy. The consequence is that very few electrons have Lorentz factors less than $\gamma'_{\rm SSA}$.

The three Lorentz factors $\gamma'_{\rm m}$, $\gamma'_{\rm c}$, and $\gamma'_{\rm SSA}$ have characteristic frequencies $\nu'_{\rm m}$, $\nu'_{\rm c}$, and $\nu'_{\rm SSA}$, which are obtained by inserting the corresponding Lorentz factor into Equation (2.12).

Each electron that radiate synchrotron emission, emits over a range of frequencies. The overall shape of the individual electron spectrum is remarkably enough independent of the electron energy. For instance, the spectral flux density (flux per unit frequency) in the low-energy tail of the spectrum is proportional to the frequency to power one third: $F_\nu \propto \nu^{1/3}$ (Blumenthal & Gould, 1970; Rybicki & Lightman, 1979).

The observed spectrum is a superposition of synchrotron spectra from all electrons at the source. Hence, the distribution of the electrons affect the shape of the observed spectrum. If the electron distribution is isotropic and in a power-law as defined in Equation (2.13), then the spectral flux varies as $F_\nu \propto \nu^{-(p-1)/2}$ (Blumenthal & Gould, 1970; Rybicki & Lightman, 1979). However, this assumes that the power-law does not change with time. Because of their synchrotron emission, the particles lose energy and cool, which alters the shape of the electron distribution. The general picture is that the particles cool quickly due to synchrotron emission down to Lorentz factor $\gamma'_{\rm c}$. Below $\gamma'_{\rm c}$, the particles are dominantly cooled by the adiabatic expansion. However, this is a slow process (in comparison) and the particles can be assumed to be static. Therefore, there are two cases depending on the position of $\gamma'_{\rm m}$ relative to $\gamma'_{\rm c}$.

Fast cooling. Electrons are in the so called the *fast cooling regime* if $\gamma'_{\rm m} > \gamma'_{\rm c}$. In this scenario. the electrons cool down quickly to $\gamma'_{\rm c}$, where the cooling stops. Thus, below $\gamma'_{\rm c}$ the spectrum is simply the combined low-energy tails from each individual synchrotron electron as all of them emits according to $F_\nu \propto \nu^{1/3}$. Between $\gamma'_{\rm m}$ and $\gamma'_{\rm c}$, the cooling alters the shape of the spectrum so that $F_\nu \propto \nu^{-1/2}$ (Sari et al., 1998). Above $\gamma'_{\rm m}$ they are continuously injected with a slope $-p$, but they also cool. The power-law injection contributes a factor of $-(p-1)/2$ and the cooling a factor $-1/2$ to the electron index. The spectral slope is therefore $F_\nu \propto \nu^{-p/2}$. In the top panel of Figure 2.1, a fast cooling spectrum is shown.

Slow cooling. Electrons are in the so called the *slow cooling regime* if $\gamma'_{\rm c} > \gamma'_{\rm m}$. In this case the electrons injected below $\gamma'_{\rm c}$ are assumed to be static due to the inefficient cooling. Without efficient cooling the spectrum is given by $F_\nu \propto \nu^{-(p-1)/2}$, which is therefore appropriate between $\gamma'_{\rm m}$ and $\gamma'_{\rm c}$. Above $\gamma'_{\rm c}$, we have to account for the cooling as well. Similarly to the fast cooling scenario, one gets $F_\nu \propto \nu^{-p/2}$. Below $\gamma'_{\rm m}$ the slope is the combined low-energy tail of $F_\nu \propto \nu^{1/3}$. The bottom panel of Figure 2.1 shows a slow cooling spectrum. For both fast and slow cooling, the flux drops steeply below the absorption frequency. *Marginally fast cooling.* In synchrotron models of the prompt emission, one needs the electrons to be fast cooling. Else it is difficult to get a sufficient amount of energy out in radiation. However, the low-energy slope of GRB spectra are much harder than what fast cooling predicts. This has been referred to as the *synchrotron line-of-death* problem (Preece et al., 1998). A slow cooling scenario could somewhat harden the low-energy slope. This has lead to the suggestion of a marginally fast cooling regime, defined as $\gamma'_{\rm c} \lesssim \gamma'_{\rm m}$ (Daigne et al., 2011). In this case, it is possible to get sufficient energy out in radiation while maintaining a harder low-energy slope. GRBs that have been fit with synchrotron models consistently show that the electrons need to be marginally fast cooling to

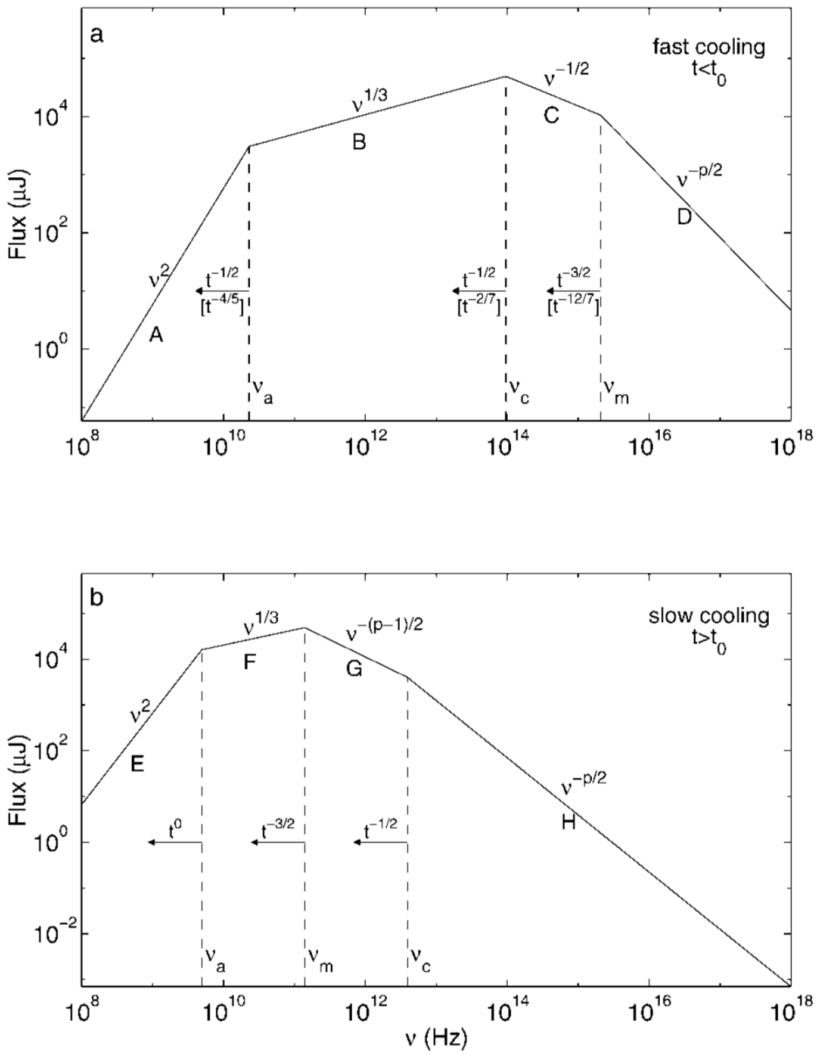

Figure 2.1. Theoretical synchrotron spectra in the fast cooling (top) and slow cooling (bottom) regimes. Below the absorption frequency (ν_a in the figure), the spectrum falls steeply. The figure also displays how the typical frequencies evolve with time. The labeling of the different slope with A to H refers to text in the original paper and is not relevant here. Figure adopted from Sari et al. (1998).

get a good fit to the data (Ravasio et al., 2018; Oganesyan et al., 2019; Ravasio et al., 2019). However, there is so far no theoretical grounds for why $\gamma'_{\rm c}$ would consistently be similar to $\gamma'_{\rm m}$. This remains a problem for theoretical synchrotron models.

Chapter 3

UHECR physics

The energies of UHECRs are incomprehensible. In the large hadron collider at CERN, particles are accelerated up to 6.5 TeV (6.5×10^{12} eV). The most energetic UHECRs can reach energies that are a million times higher. The ratio is the same as the width of a fingernail ($\lesssim$ 1 cm) to the height of Mount Everest ($\lesssim$ 10 000 m). UHECR can therefore help us study particle physics at energies that would be otherwise unattainable.

The Chapter is divided as follows. In Section 3.1 I describe how CRs are (most likely) accelerated. In Section 3.2, I give more detail about the spectrum of UHECR. Section 3.3 and 3.4 give constraints on the local magnetic field to accommodate UHECFR acceleration and in Section 3.5, I derive the minimum total energy of possible sources.

3.1 Cosmic ray acceleration

In 1949, a famous paper was published by Enrico Fermi (Fermi, 1949). With the discovery and continuous study of CRs, a standing problem was how these particles were accelerated. The common view at the time was that the particles where galactic. However, a competing hypothesis, voiced by Hannes Alfvén among other, was that CRs mainly originated from the Sun, where they could be contained in the Sun's magnetic field. The argument was that it would require a huge amount of energy to accelerate CRs if they existed all throughout galactic space, as no efficient acceleration mechanism was known. In his paper, Fermi (1949) outlines the process that is now known simply as *Fermi acceleration*.

The principle idea is that space is permeated by magnetic fields, which will randomly cluster into more and less dense areas. If a CR interacts with a patch of denser magnetic field (denser clouds as called by Fermi)

it can interact in the magnetic field lines and be reflected. The process can result in either an energy gain or an energy loss for the particle. The outcome depends on in which direction the magnetic cloud was moving, with the particle gaining the most energy in a head-on collision. On average the particle encounters more clouds moving towards it than away from it, for the same reason that you see more people walking passed you in the opposite direction when walking on a footpath than the number of people you overtake. Statistically, this leads to a net gain of energy for the particles. Furthermore, this process naturally produces a power-law in energy similar to that of the cosmic ray spectrum (Figure 1.2).

While it was not Fermi's original application, the same acceleration phenomenon can be applied to shocks (Bell, 1978). In shock physics, one often calls the material that has not yet crossed the shock front for the *upstream* and similarly material that has passed the shock is called the *downstream*. Over a shock front, there is a discontinuous jump of several macroscopical quantities. The relationship between the upstream and downstream quantities are described by the shock-jump conditions, or the Rankine-Hugoniot equation (Rankine, 1870; Hugoniot, 1887a,b).

Velocity jump

One of the discontinuous properties over a shock front is the velocity of the bulk flow. That the velocity changes is most easily realized in the scenario when the shock is driven into an upstream at rest. In this case, the particles have zero net velocity in the upstream, but are swept along by the shock as it passes. Thus, in the downstream the particles have a non-zero mean velocity in the same direction as the shock. As shocks are often identified as having no spatial extent, this lead to a discontinuous jump of the velocity over the shock front. In reality, shocks always has some finite width over which the velocity indeed changes continuously. In shock physics, it is often easiest to work in the frame where the shock is stationary (see Figure 3.1). In this frame, the upstream material flows towards the stationary shock with a larger velocity than the downstream material flows away from the shock.

In Fermi acceleration across a shock, also known as *diffusive shock acceleration*, charged particles scatter off of magnetic irregularities in the up- and downstream of the shock (Figure 3.1). A particle entering the downstream has some probability of being reflected back into the upstream by magnetic turbulence. In the upstream, it encounters a fast, moving flow coming towards it (in the rest frame of the shock) and is reflected back. A

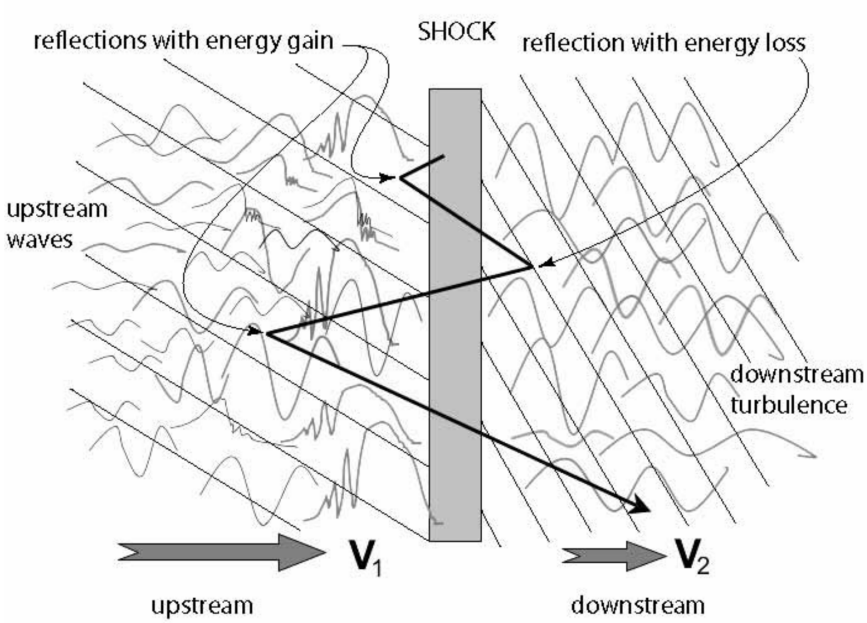

Figure 3.1. Schematic picture of diffusive shock acceleration. The motion of the charged particles back and forth across the shock front generate magnetic instabilities, which in turn can scatter the particles. Each crossing of the shock gives a net energy gain of the particle. In each iteration, the particle can either cross the shock once more or diffuse downstream. Figure adopted from Treumann & Jaroschek (2008).

particle can cross the shock front many times through this mechanism. Because of the velocity difference between the upstream and the downstream, the particle gains energy in each iteration. Furthermore, as the particle has some probability of exiting the acceleration process each time it returns to the downstream, the distribution of charged particles is a power-law (Bell, 1978). The process of diffusive shock acceleration is today viewed as the most promising acceleration mechanism of UHECR.

3.2 Spectrum

The CR spectrum (Figure 1.2) is remarkable in that it is so unremarkable. Over more than ten orders of magnitude, it extend with an almost perfect power-law. The single power-law hints that all CRs are produced through the same acceleration mechanism and the slope of the spectrum

agrees quite well with that predicted by diffusive shock acceleration. However, some features exists. Of specific interest to this thesis is the ankle, which is a flattening of the CRs spectrum above a few 10^{18} eV. With a zoom-in at the relevant energies the feature is clearly visible (Figure 3.2). The interpretation is that at these energies, the Larmor radius of the CRs (see Equation (3.1)) becomes so large that they cannot be contained by the galactic magnetic field (see the marked regions for the galactic disk and halo in Figure 3.3). Hence, the UHECR that are produced in our galaxy diffuse away. Similarly, the extragalactic UHECR produced can diffuse out of their respective host galaxy and arrive at Earth. This causes the shift in the spectrum.

At energies above $\sim 10^{20}$ eV, there is a sharp cut-off in the spectrum. Such a cut-off was independently predicted before is was observed by Greisen (1966); Zatsepin & Kuz'min (1966). It is known as the GZK cut-off after the initials of the original authors Greisen and Zatsepin & Kuzmin. The reason for the abrupt fall in flux is that space is permeated by a low-energy photon background called the cosmic microwave background. It is a remnant from the early days of the Universe when radiation decoupled from matter (it is a similar effect to the emission from the photosphere described in Section 4.2.2 but on the scale of the whole Universe). UHECR of sufficient energy can interact with these low-energy photons and create pions. For this process to work, the center-of-mass kinetic energy of the CR and photon has to be higher than the pion rest mass energy. For the cold photons of the cosmic microwave background this requires a CR energy of $\sim 10^{20}$ eV. Thus, we do not observe UHECRs with energies beyond this even if their initial energy was higher, as they lose their excess energy while propagating towards Earth.

3.3 Hillas criterion

Magnetic fields are ubiquitous in the Universe. The magnetic fields strength that are present cover an impressive range, from a few μG in the interstellar medium to $\sim 10^{15}$ G around fast, rotating neutron stars called magnetars. In many astrophysical situations, the magnetic fields play a crucial role in the dynamics and observational signal of the system.

Charged particles in magnetic field gyrate around magnetic field lines. The radius of the circle of gyration is called the *Larmor radius*. In the relativistic case it is given by

$$r_{\mathrm{L}} = \frac{E}{|q|B} \tag{3.1}$$

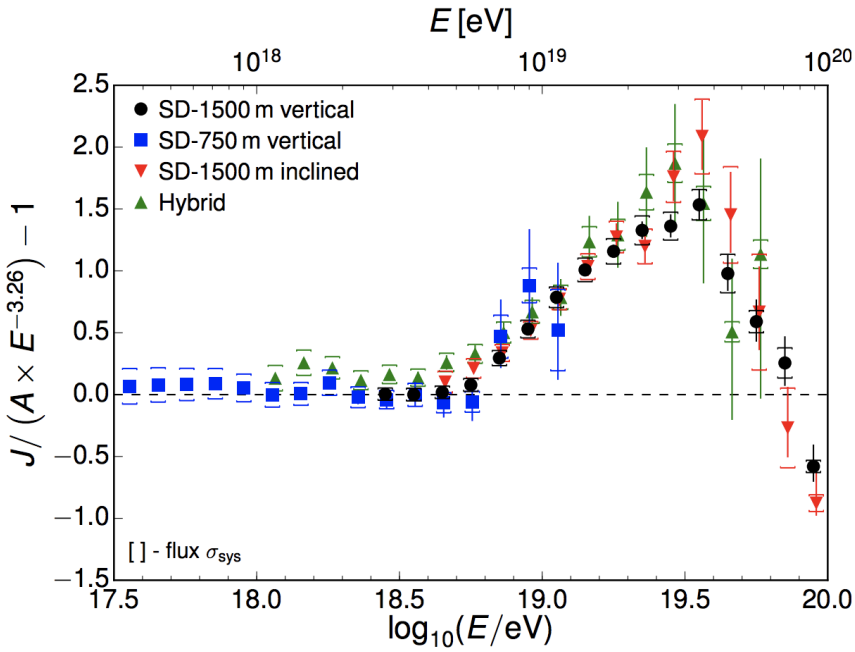

Figure 3.2. Zoom-in on the CR spectrum at the highest energies. The y-axis has been multiplied by $E^{3.26}$ for the feature to appear more prominently. The GZK cut-off causes the drop in flux after $\sim 10^{19.5}$ eV. The different colored data points correspond to different configurations of the Pierre Auger experiment as described in The Pierre Auger Collaboration et al. (2015). Figure adopted from The Pierre Auger Collaboration et al. (2015).

where $E = \gamma mc^2$ is the particle energy, $|q|$ is the absolute value of the particle charge, and B is the magnetic field strength. Quite intuitively, Equation (3.1) tells us that higher energy increases the Larmor radius (less tightly bound to the magnetic field lines), while stronger magnetic fields and higher charge decreases it (more tightly bound).

The so-called *Hillas criterion* Hillas (1984) gives a simple, necessary requirement for potential UHECR sources. Accelerating particles to UHECR takes time. The higher energy the particle obtains, the larger Larmor radius it gets. To continue the acceleration process, the particle must always be confined to the region or system in which the acceleration takes place. Thus, the magnetic field needs to be sufficiently strong and/or the system size sufficiently large. Given that the observed energies reach $E = 10^{20}$ eV, it is easy to estimate what sources have the correct properties in terms of size and magnetic field. For instance, a magnetic field strength of $B = 10^3$ G requires a system size of $r = 3 \times 10^{14}\ E_{20}/B_3$ cm to contain protons. In Figure 3.3, I show the original Figure as it appears in Hillas (1984). It is evident that this simple argument rules out many astrophysical events as UHECR sources. GRBs are not marked in the Figure, but they have no problem of satisfying the Hillas criterion.

3.4 Magnetic field strength

The Hillas criterion outlined in Section 3.3 gave an estimate for the magnetic field strength required to accelerate UHECRs. However, it is possible constrain the magnetic field strength further. The analysis follows that of Waxman (1995a) who was early in suggesting that GRBs could be the accelerators of UHECRs. The idea is simple. For particles to be accelerated to a specific energy E, the time it takes to reach that energy should be shorter than the typical times at which the particle loses energy.

In Section 2.5, I presented that electrons lose energy mainly due to their synchrotron emission and the adiabatic expansion of the jet. When regarding CRs, one also need to account for the energy losses from the interactions the surrounding photons. Below, I give a brief derivation of the typical time scale of energy loss due to photohadronic interactions.

Along the path of a relativistic CR, the probability P of a photohadronic interaction across a length $dr' = c\,dt'$ is $P = n'\sigma_{p\gamma}c\,dt'$, where n' is the comoving photon density and $\sigma_{p\gamma} \sim 10^{-28}$ cm^2 is the photohadronic cross section. The number of photons to interact with can be estimated from the observed luminosity L_γ. If the characteristic observed energy is $\langle\varepsilon\rangle$, then the observed luminosity is $L_\gamma \sim 4\pi r^2 cn' \langle\varepsilon\rangle\,\Gamma$. The cosmic rays lose roughly

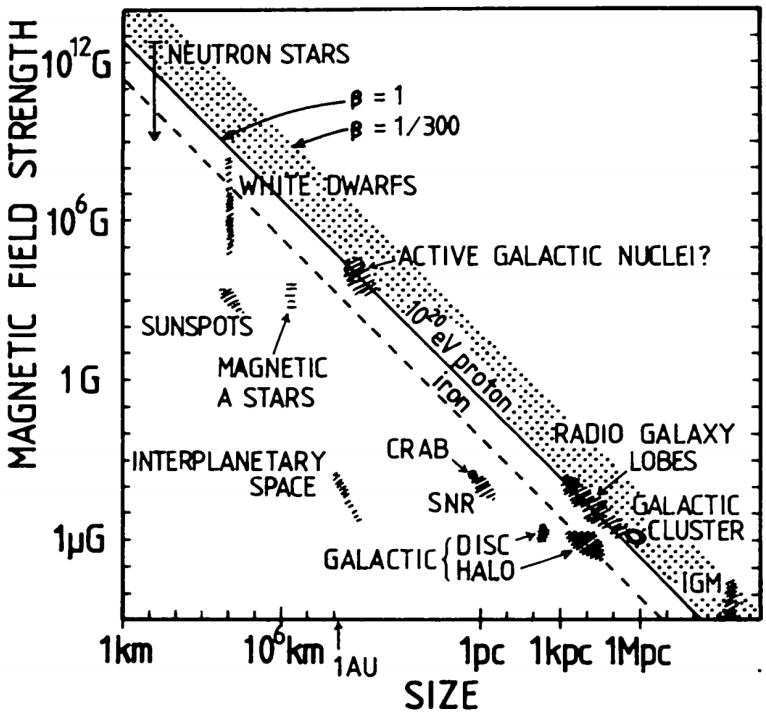

Figure 3.3. Original Figure of the Hillas criterion as it appears in Hillas (1984). The smaller the size of the system the larger the magnetic field strength needs to be in order to contain the particles. To accelerate the highest energy UHECR requires that the source can be placed somewhere in the shaded area. GRBs are not shown but satisfies the criterion.

20% of their energy in each collision (Mücke et al., 1999). Thus, we get the timescale for photohadronic losses

$$t'_{p\gamma} = \frac{20\pi r^2 \langle \varepsilon \rangle \Gamma}{\sigma_{p\gamma} L_\gamma}. \tag{3.2}$$

The energy loss timescales given by Equations (2.9), (2.19), and (3.2) should be compared to the time it takes the particle to gain energy. The acceleration time scale (in the comoving frame) to reach an energy E is given by

$$t'_{\rm acc} = \frac{E}{\eta Z e c B' \Gamma}. \tag{3.3}$$

The acceleration time scale is proportional to the energy obtained in the comoving frame E'; the longer time available for acceleration, the higher energies can be reached. The energy E is the observed energy and must therefore be divided with the Lorentz factor of the outflow Γ to get the energy in the outflow frame. The acceleration time is further inversely proportional to the charge of the particle Ze, where Z is the charge number and e is the elementary charge, and to the magnetic field strength B'. This implies that more charged particles and stronger magnetic fields lead to shorter acceleration times. The factor η is called the acceleration efficiency and is a dimensionless proportionality constant. The true value of η is unfortunately not known but it somewhere of the order $\eta \sim 0.1$ (Protheroe & Clay, 2004; Rieger et al., 2007; Caprioli & Spitkovsky, 2014).

Once all timescales are defined, it is straight forward to check what values of the magnetic field are required to satisfy the condition $t'_{\rm acc} < \min[t'_{\rm sync}, t'_{\rm ad}, t'_{p\gamma}]$. The conditions on B' are shown in Figure 3.4, taken from Paper II. The methodology of constraining the magnetic field strength presented here is used in Paper I and for the prompt phase in Paper II.

3.5 Energy budget

For a specific type of astrophysical event to be the main sources of UHECRs, they need to output sufficient energy in UHECRs to support the flux observed on Earth. Because of the very low statistics at the high-energy end of the CR spectrum, the energy output needed is quite uncertain. Current estimates put the injection rate at roughly $E(dQ_{\rm UHECR}/dE) \sim 10^{44}$ erg Mpc^{-3} yr^{-1} (Waxman, 1995b; Katz et al., 2009; Murase & Takami, 2009; Zhang et al., 2018).

This should be compared to the event rate of the potential sources; if the sources are more common, they each have to contribute less to the UHECR

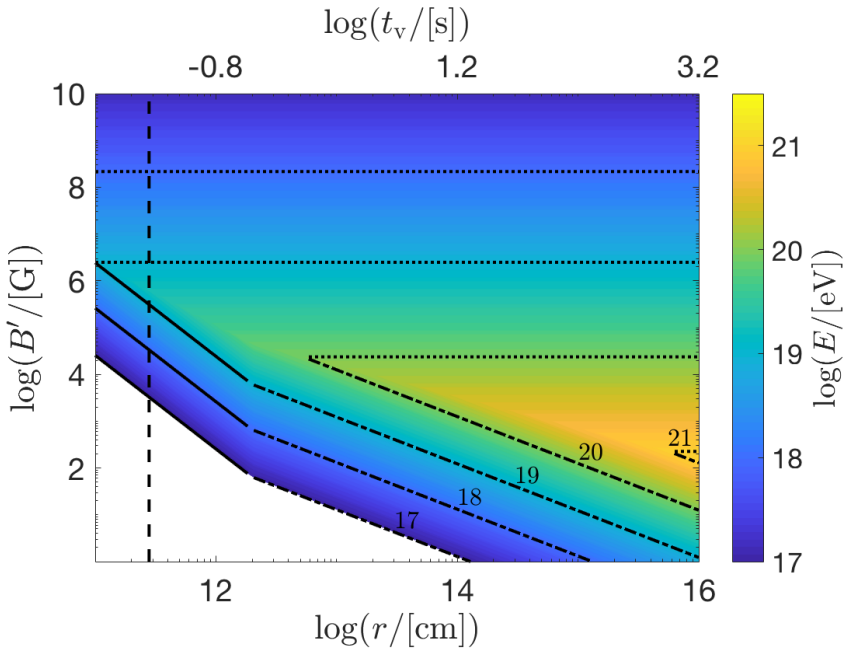

Figure 3.4. Allowed parameter space for B' as function of r and E for bulk Lorentz factor $\Gamma = 10$. The color bar shows $\log(E/[\mathrm{eV}])$ for iron ($Z = 26$) and the vertical dashed line shows the photosphere (see Section 4.2.2). The top x-axis shows the minimum variability time $t_\mathrm{v} = r/2\Gamma^2 c$. The dotted lines show the limits on B' obtained from $t'_\mathrm{acc} < t'_\mathrm{sync}$, the dot-dashed lines show the limits from $t'_\mathrm{acc} < t'_\mathrm{ad}$, and the solid lines show the limits from $t'_\mathrm{acc} < t'_{p\gamma}$, all for integer values of $\log(E/[\mathrm{eV}])$ as indicated in the plots. Numerical values used are $L_\gamma = 3 \times 10^{46}$ erg s^{-1}, $\eta = 0.1$, and $\langle\varepsilon\rangle = 5$ keV. Figure adopted from Paper II.

injection. For this thesis, the event rates of GRB is most important. However, the argument holds for any potential UHECR source. The apparent local event rate of low-luminosity GRBs (llGRBs) $R_{\rm LL,app}$ is estimated to be 10^2–10^3 Gpc^{-3} yr^{-1} (Soderberg et al., 2006; Pian et al., 2006; Toma et al., 2007; Murase & Takami, 2009; Sun et al., 2015). Apparent here refers to the fact that if llGRBs are beamed with a jet, the event rate could be higher (as we would only observe the ones with jets pointing towards us). However, as explained in Section 4.1.4, llGRBs are probably not highly collimated. The estimated event rate of llGRBs is also uncertain due to the few llGRBs detected so far.

The event rate of high-luminosity GRBs, or canonical GRBs, is generally believed to be lower. Again, this is uncertain. This time, the uncertainty stems from the opening angle of the jet. Estimates put the rate around $R_{\rm HL} = 1$–10 Gpc^{-3} yr^{-1} (Pian et al., 2006; Soderberg et al., 2006; Sun et al., 2015), although I note that Guetta & Della Valle (2007) got a higher event rate of > 100 Gpc^{-3} yr^{-1}. Here, the rate is not the apparent rate as high-luminosity GRBs are known to be relativistic and beaming has been accounted for.

Once UHECR energy injection rate and local rate of low and high-luminosity GRBs is given, one can calculate how much energy on average every event needs to release in UHECR:

$$Q_{\rm UHECR}/R_{\rm LL,app} = 10^{50}\, Q_{\rm UHECR,44} R_{\rm LL,app,3}^{-1}\ {\rm erg} \tag{3.4}$$

for llGRBs and

$$Q_{\rm UHECR}/R_{\rm HL} = 10^{52}\, Q_{\rm UHECR,44} R_{\rm HL,1}^{-1}\ \ {\rm erg} \tag{3.5}$$

for high-luminosity GRBs. The energy budget requirement is used in Paper II.

Chapter 4

GRB physics

As mentioned in the Introduction, GRBs are bright, short flashes of gamma-ray radiation that can be seen by satellites in outer space. They have baffled scientists for for over half a century and there are still many things that remain unknown. They are so difficult to study due to their short duration and wide variety of observational properties. Theoretical and observational effort led to the detection of the afterglow in 1997 (Rees & Mészáros, 1994; Costa et al., 1997), which is lower-energy radiation that last for weeks to months after the explosion. To differentiate between the two phases, the first flash of bright gamma-rays is nowadays called the prompt phase.

In this Chapter, I give a brief overview of GRB physics. In Section 4.1, I go through some characteristics of GRB observations and why they are so hard to classify. In Section 4.2, I outline some theoretical models regarding the prompt phase. Lastly, in Section 4.3 I describe the afterglow emission.

4.1 Observations

Before going into some of the theoretical GRB models in Section 4.2, I outline some of the most important observational properties of GRBs in this Section.

4.1.1 Light curves

One of the main difficulties in characterizing the prompt emission of GRB, together with the short duration time, is the vast differences in observed light curves. GRB light curves come in a great variety of shapes with no coherent or periodical behavior. There exists those with a single sharp peak and those that are double or triple peaked. Some consists of a smooth single

pulse with no variability, while yet others are very chaotic with seemingly no regularity. A selection is shown in Figure 4.1, where the diversity is clearly visible. This poses a challenge for any successful GRB model, which must be able to reproduce a large range of observations.

A second important piece of information from the light curves is the short variability times observes. GRBs can exhibit variability times as short as $\sim$ 10 ms (see for instance GRB 910711 and 940210 in Figure 4.1). Such short variability times indicated that the emission region had to be very compact, with lots of high-energy photons that should pair produce. This problem was coined the *compactness problem* and was an early motivation for why GRB outflows were relativistic.

Compactness problem

The light travel time across a spherical shell with radius R is given by R/c. Imagine that an instantaneous pulse of light is emitted from a spherical blast wave with radius R. The light from the region closest to us would reach us first, followed by the light emitted by the more distant parts of the sphere. The observed signal would be a pulse with duration $t_{\rm v} \sim R/c$, i.e., the initial, instantaneous pulse has been "smeared out". An observed variability time of only $t_{\rm v} \sim 10$ ms should indicate an emission radius of $R \sim 3 \times 10^8$ cm. However, such a small emission radius is problematic. All the observed high-energy photons would be contained in a small region resulting in a high density of energetic photons. The optical depth for pair-production for typical GRB luminosities and photon energies would be huge and so these photons should not escape. Yet, we do observe them.
This is one of the early arguments for the outflows of GRBs to be relativistic (Ruderman, 1975; Schmidt, 1978). In a relativistic outflow with Lorentz factor Γ, the variability time is reduced by a factor of Γ^2. Thus, $\Gamma \sim 100$ the emission could occur at $R \sim t_{\rm v}\Gamma^2 c \sim 3 \times 10^{12}\ t_{\rm v,-2}\ \Gamma_2$ cm instead. Furthermore, a relativistic outflow means the observed photons are blueshifted, and their energy in the rest frame of the outflow is reduced by a factor $\sim \Gamma$. Thus, the typical comoving photon energies are much lower, reducing the number of available photon-pairs that can pair-produce.

4.1.2 Short versus long GRBs

The duration of the prompt emission of a GRB is most commonly measured by the T_{90} parameter. The T_{90} of a GRB is defined as the time interval between which 5% and 95% of the total fluence is detected. It is obvious

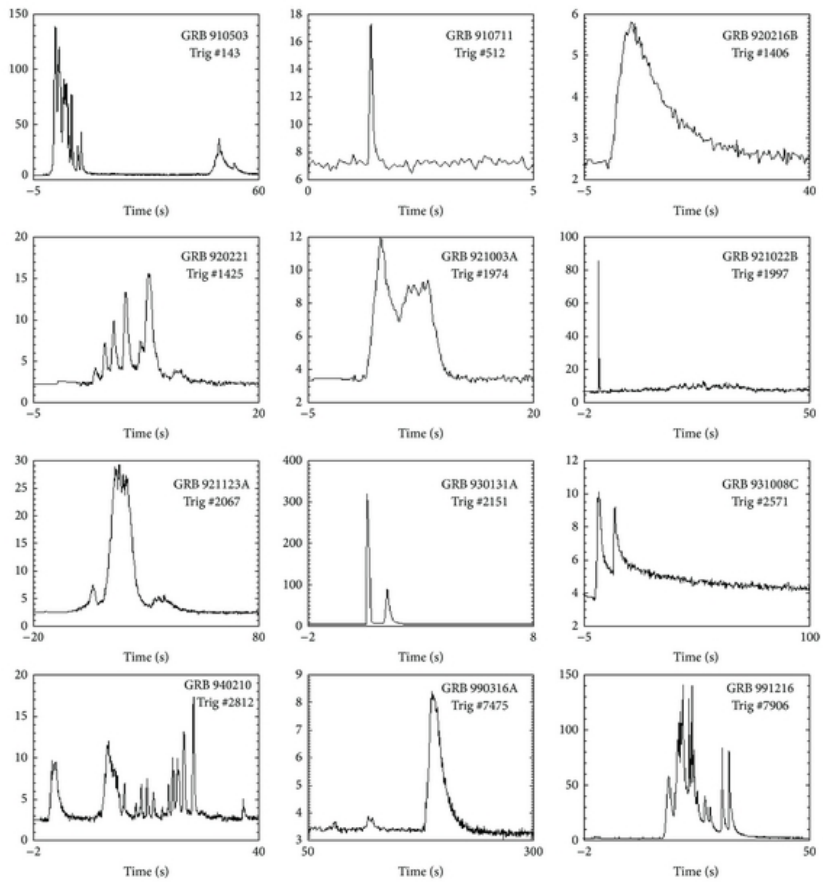

Figure 4.1. A selection of twelve GRB light curves to show their wide variety of shapes. This makes GRBs difficult to chategorize. Some also show very rapid variability. Figure adopted from Pe'er (2015), created by Daniel Perley using data from the public BATSE archive (`http://gammaray.msfc.nasa.gov/batse/grb/catalog/`).

how such a definition can be misleading. Looking at the top left panel of Figure 4.1, this burst was cataloged with a $T_{90} = 51$ s (Fishman et al., 1994). Without access to the actual light curve, this number clouds the fact that for most of that time there was no observed emission. Regardless of the drawbacks of the T_{90}-parameter, it was realized in the BATSE-era that the T_{90}-distribution of GRBs was bimodal (Kouveliotou et al., 1993). That is, the sample of GRBs could be subdivided into short GRBs with a mean duration of ~ 0.3 s and long GRBs (with a mean duration of ~ 26 s. The separation between the two populations occur at roughly 2 s. Kouveliotou et al. (1993) also showed that the two population had different hardness ratios, which supported the hypothesis that they were indeed two separate classes of transients. Short GRBs were found to be harder than long GRBs.

It has now been firmly established that the two types of GRBs are associated to different progenitors. Long GRBs have been observed in coincidence with SN explosions of type Ib/c (Galama et al., 1998; Hjorth et al., 2003; Campana et al., 2006; Pian et al., 2006; Starling et al., 2011; D'Elia et al., 2018), while the famous event GRB 170817A confirmed that at least some short GRBs are created between the merger of two neutron stars (Abbott et al., 2017a,b).

4.1.3 Spectra

The observed spectrum of GRB are historically most frequently fitted with the *Band function* (Band et al., 1993). It is a phenomenological function without any physical meaning. While the original idea behind the Band function was to not introduce any biases by fitting a preferred physical model, the GRB community is now more and more leaning towards physical fitting. The reason is that physical interpretation based on the result of fits done with the Band function can be misleading.

The original Band function is a bit cumbersome and unintuitive. However, it resembles two power-law segments that has been smoothly connected. A broken power-law function can be written as (compare with the single power-law in Equation (2.13)

$$\frac{dN}{dE} = A \begin{cases} \left(\frac{E}{E_0}\right)^{-\alpha} & E < E_0, \\ \left(\frac{E}{E_0}\right)^{-\beta} & E > E_0. \end{cases} \tag{4.1}$$

Similarly to the Band function, the function in Equation (4.1) has 4 unknown parameters: the low-energy spectral slope α, the high-energy spectral slope β, the peak-energy E_0 and the overall normalization A. Typical parameters are $\alpha \sim -1$, $\beta \sim -2$ and $E_0 \sim$ few 100 keV. The normalization A of the observed spectrum varies with the distance to the source and the

unknown intrinsic brightness of the GRB. It is easy to see that for the typical values of α and β the peak energy, or break energy, does not correspond to a peak of the function given in Equation (4.1). However, GRB spectra are most commonly plotted in νF_ν spectra, in which case the low- and high-energy spectral slopes α and β are increased by 2. Then, E_0 indeed becomes a peak in the spectrum.

Historically, many deductions of GRBs has been made from the specific parameter values of α, β, and E_0. However, given the way that the data is analyzed, this can lead to incorrect conclusions regarding the physics. A GRB detector registers counts in bins. Idealized, bin number corresponds to energy and each count to one detected photon of that energy. In reality, lots of different things leads to uncertainty of the data. Photons scatter in the detector, which means that a single photon can be detected as two separate counts or it may escape after the scattering, thus depositing only a fraction of its energy in the detector. Furthermore, there is uncertainty in the readout and two simultaneously incoming photons might be registered as one.

To convert the counts and bins into the information that we want, (i.e., this much energy deposited during this time at these frequencies) one uses a forward-folding technique. This works as follows. First, a model spectrum to mimic the true spectrum of the source is chosen. Such a model spectrum is for instance the Band function with specified parameters α, β, E_0, and A. This model spectrum is then run through the response matrix of the detector. The response matrix outputs a prediction of the number of counts in each bin one would observe given that the incoming spectrum was the model spectrum. One can then make a statistical comparison of this output to the actual data. The process can then be repeated with slightly different parameter values to see if a better fit is obtained. If done enough times, one can find the best fit values of α, β, E_0, and A. However, the fit relies on the fact that the true spectrum was a Band function, which is of course not the case since the Band function is a only a mathematical concept. The big caveat is that different models, with different physical interpretations, can give equally good fits to the data once forward folded. Unfortunately, this is the only way the data can be analysed, since the response matrix of the detectors are non-invertable (Pe'er, 2015).

4.1.4 Low-luminosity GRBs

In 1998, Galama et al. (1998) reported a SN in the error box region of GRB 980425. They estimated the chance coincidence of the two events occurring so close to each other in space and time to be less than 1 in 10^4. Thus, the two events were most likely correlated. This was the first time an association

between GRBs and SN had been observed. Furthermore, while the GRB seemed common enough in itself, once the very short distance to the event was determined it was revealed that GRB 980425 was roughly four orders of magnitude less energetic than typical GRBs ($E \lesssim 10^{48}$ erg) (Galama et al., 1998).

With time, more and more detections similar to GRB 980425 were made (e.g., GRB 031203 (Sazonov et al., 2004), GRB 060218 (Campana et al., 2006; Pian et al., 2006), GRB 100316D (Starling et al., 2011)). All of these were very close by, associated with luminous SN type Ib/c, and all of them were much less luminous than standard high-luminosity GRBs. With more detections, the idea emerged that the low-luminosity GRBs (llGRBs) might be a separate class of transients, intrinsically different than the previously known high-luminosity GRBs. One of the compelling arguments for this idea was that the rate of llGRBs seemed higher than the rate of canonical, high-luminosity GRBs. The lower luminosities of llGRBs mean that they are only detectable in a small volume in our local universe unlike canonical GRBs that can be seen from incredibly far away. Thus, even though detections of llGRBs are much more scarce than canonical GRBs, their intrinsic rate can still be higher. Indeed, rate estimates seem to indicate that llGRBs are at least ten times more common, indicating that the two classes can have different origins (Pian et al., 2006; Soderberg et al., 2006; Guetta & Della Valle, 2007; Sun et al., 2015, see also Section 3.5).

llGRBs are generally believed to be mildly relativistic outflows with bulk Lorentz factor in the order of a few (Soderberg et al., 2006). If they launch a jet similarly to high-luminosity GBRs or not is uncertain (Campana et al., 2006; Fan et al., 2006; Toma et al., 2007). One interpretation of llGRB prompt emission is that it is caused by a shock breakout from the progenitor star. In a SN explosion, fast material is launched outwards from inner parts of the parent star generating a shock wave. As the shock travels faster than the speed of sound, the outer layers of the star are initially unaware and unaffected by the internal explosion taking place. A shock breakout is when the internal shock wave reaches the outer boundary of the star, resulting in flash of X-ray radiation. That llGRBs can be the signature of a mildly relativistic shock breakout has been advocated by several authors (Campana et al., 2006; Waxman et al., 2007; Nakar & Sari, 2012).

4.2 Prompt emission

One of the big question in GRB research today is what is causing the emission of the variable prompt emission that we observe. In this Section, I briefly go through some of the leading models.

4.2.1 Fireball model

A consequence of the compactness problem described in Section 4.1.1 is that the observed radiation cannot be emitted in the close vicinity of the progenitor. Furthermore, the emission must be emitted by a source moving with relativistic velocities towards us. Both of these requirements are met by the fireball model.

GRBs are most often described using the fireball model (Paczyński, 1986; Goodman, 1986; Rees & Mészáros, 1992, 1994). In the fireball model, an initial amount of energy (most likely gravitational or rotational) is converted into copious amounts of radiation. Close to the progenitor the outflow is optically thick, which means that the photons cannot escape. The photons collide with the material in the outflow, transferring their energy to the matter. As the ejecta moves outwards, it expands and cools with the internal energy of the photons being converted into bulk kinetic energy of the outflow. At a certain point, given that the ejecta is still optically thick, the photons will have transferred all of their energy into bulk kinetic energy and the outflow stops accelerating and coasts. The outflow is now in the coasting phase, moving with a terminal bulk Lorentz factor $\Gamma = E/Mc^2$, where E is the total energy released in the burst and M is the matter in the outflow.

Although the description regarding the relativistic fireball is spherical, it is equally valid if the emission occurs in a collimated jet. If one looks down the funnel of a relativistic jet with bulk Lorentz factor Γ, one would mainly see emission coming from a solid angle cone with opening angle $\theta \sim 1/\Gamma$ due to relativistic beaming. As long as θ is smaller than the opening angle of the jet, the observer is limited to seeing only the fraction of emission that is being beamed towards them. As such, the observer cannot differentiating between a beamed, collimated outflow and a spherical one. Thus, the framework of spherical symmetry is valid. One often speaks of *isotropically equivalent* energy or luminosity in such a case, which means the energy the burst would have, if the observed radiation was emitted over a whole sphere. The true energy in the jet is lower by the fraction of the solid angle subtended by the jet compared to the whole sky (4π).

To generate the GRB emission that we observe, some physical process must tap into the kinetic energy of the outflow, re-converting it into high-energy radiation. Currently, there is no consensus within the scientific community on how this is done. I outline of the most prominent models below.

4.2.2 Photosphere

Initially when the ejecta is launched, the outflow is optically thick. The existing photons interacts with the electrons, positrons, and baryons in the

outflow and cannot escape. As the outflow moves further out, it expands, leading to a larger mean separation between the particles. At some point, it will become more likely for a photon to escape to infinity than to interact another time. Beyond this radius, the photons can more or less stream freely and are able to reach us as distant observers. Mathematically, this occurs when the optical depth τ becomes unity, which is defined as the *photospheric radius* $r_{\rm ph}$. For typical GRB-parameters $r_{\rm ph} \sim 10^{11}$–10^{13} cm (Rees & Mészáros, 2005).

As the initial ejecta is optically thick, release of the trapped photons at the photosphere is inevitable. Thus, photospheric emission is always present but it may not be the dominant contribution to the prompt emission. Interpreting the prompt emission as photospheric radiation was suggested early on (Paczyński, 1986; Goodman, 1986). However, these early papers predicted that the emitted spectrum would be close to a blackbody, as the photons would have had time to completely thermalize before reaching the photosphere. A blackbody spectrum is very narrow, unlike the typical, much broader observed GRB spectra. Therefore, the idea was largely abandoned.

An observed photospheric spectrum from a GRB can never be as narrow as a blackbody. There are several effects that will broaden the spectrum. Due to the relativistic velocities of the outflow, the intrinsic blackbody spectrum has to be Lorentz transformed into the observer frame, increasing the spectral width (Beloborodov, 2010). Furthermore, the notion of a photospheric radius is a simplification. The escape of a photon is a statistical process, which means that photons escape at a variety of radii. Indeed, the emission occurs over more than an order of magnitude in radius (Pe'er, 2008; Lundman et al., 2013). As the radius increases, the outflow adiabatically cools and the temperature drops. The observed spectrum is thus a superposition of blackbodies with different temperatures from the photons emitted at different radii. Angular effects also broaden the spectrum. The optical depth towards the observer is different depending on the angle to the line of sight, again leading to different temperature blackbodies being emitted (Abramowicz et al., 1991; Pe'er, 2008; Lundman et al., 2013). As such the photosphere is rather a volume than a radius. A spectrum consisting of many different temperature blackbodies is often called a *multicolored blackbody*.

All three processes mentioned above inevitably broaden the spectrum, even if the photons are completely thermalized. If energy is dissipated when the ejecta is still optically thick, the spectrum released at the photosphere might not resemble a blackbody. Energy dissipation below the photosphere can occur through turbulence, shocks, re-collimation etc. Indeed, simulations show that the outflows below the photosphere are very turbulent, so sub-photospheric dissipation is expected (Lazzati et al., 2013).

Some caveats of the photospheric model is that it cannot account for the majority of GRBs observed without invoking energy dissipation below the photosphere. Some examples of spectra with a clear photospheric component exists in the literature (Ryde et al., 2010, 2017) but such examples are rare. Another problem is regarding the typical variability times observed, which are most commonly around ~ 1 s. For typical values $r_{\rm ph} \sim 10^{12}$ cm and $\Gamma \sim 100$, the predicted variability time is only $t_{\rm v} \sim 3$ ms.

4.2.3 Internal shocks

How the gravitational energy released close to the progenitor results in the launching of a collimated jet is still not well understood. However, the jet launch is expected to occur over some finite amount of time. It is quite plausible that some physical properties of the jet will vary during this time. If, say, the baryonic mass M varies but the radiation energy E stays constant, then the terminal Lorentz factor Γ will also vary across the outflow according to $\Gamma = E/Mc^2$. The different velocities can result in internal collisions. These can be relativistic in the frame of the outflow given large enough fluctuation in M (Rees & Mészáros, 1994). The collision would occur in the optically thin region above the photosphere but before the ejecta is substantially decelerated by the external medium. The internal shocks dissipates the kinetic energy of the outflow, converting it to internal energy behind the shock. With magnetic fields likely present, either from the progenitor itself or generated in the turbulent downstream, the charged particles emit synchrotron radiation.

A power-law distribution of electrons in a magnetic field naturally produces a broad spectrum through synchrotron emission (see Section 2.5). Therefore, it gained popularity in explaining the typically broad GRB spectra. One major drawback of synchrotron models was pointed out by Preece et al. (1998). The low-energy slope for a large fraction of bursts is harder than what theoretical synchrotron models predict. The term *synchrotron line of death* was coined and remains to this day a challenge for synchrotron models of prompt emission.

Lately, it has been shown that the problem might mot be as bad as originally thought. Several bursts with prompt emission previously deemed incompatible with synchrotron radiation has been shown to be possible to fit with a synchrotron model, if this model is fit directly to the data (Burgess et al., 2018). The apparent discrepancy arises from the non-linearity of the response matrix of the available instrument, as explained in Section 4.1.3. Various other papers recently published also report good agreement of the data with expectations from synchrotron emission, using either empirical functions (Ravasio et al., 2018, 2019) or fitting theoretical synchrotron

models directly to the data (Oganesyan et al., 2019). However, several questions remain as the best fit parameters found in the aforementioned papers are often in tension with current estimates. Another problem is that the emitting electrons are consistently found to be marginally fast cooling (see Section 2.5), something which is not predicted theoretically.

4.2.4 External shocks

In the framework of the fireball model, the outflow will move with constant, relativistic velocity once the radiation pressure has been converted into kinetic energy. While space is mostly empty, it is not a vacuum, which means that the ejecta eventually has to slow down. The deceleration will occur once the swept-up mass energy is comparable to E/Γ^2 (Rees & Mészáros, 1992)

$$E = \frac{4\pi r_{\rm dec}^3}{3}\rho_{\rm cbm}c^2\Gamma^2, \tag{4.2}$$

where $r_{\rm dec}$ is the deceleration radius of the outflow and $\rho_{\rm cbm}$ is the mass density of the circumburst medium.

Deceleration radius

An intuitive way of arriving at Equation (4.2) is as follows. The total observed energy of the relativistic flow is $E = \Gamma Mc^2$, where M is the total mass of the outflow. The total energy in the rest frame of the outflow is just the mass energy $E' = Mc^2$ or $E' = E/\Gamma$. In the outflow frame, the stationary outflow is continuously being bombarded by incoming particles with an energy density of $\Gamma\rho_{\rm cbm}c^2$. The outflow will be unperturbed until the pile up of incoming energy has become comparable to the rest mass of the outflow. At this point, the outflow starts to be "dragged along" by the incoming particles (i.e., decelerated in the observers frame). Accounting for the total swept up volume once the deceleration occurs of $4\pi r_{\rm dec}^3/3$, we obtain Equation (4.2).

As the relativistic ejecta is being pushed into the circumburst medium an external shock wave form. Similarly to the case of internal shocks, the shock wave converts the kinetic energy of the outflow into internal energy of the particles. Given that magnetic fields are present, the electrons will lose their energy to synchrotron radiation.

As with photospheric emission, external emission is something that is inevitably present in GRBs. However, as a mechanism for explaining the prompt phase it has been largely abandoned. Typical values of $r_{\rm dec} \sim 10^{16}$ cm is impossible to reconcile with the shortest observed variability

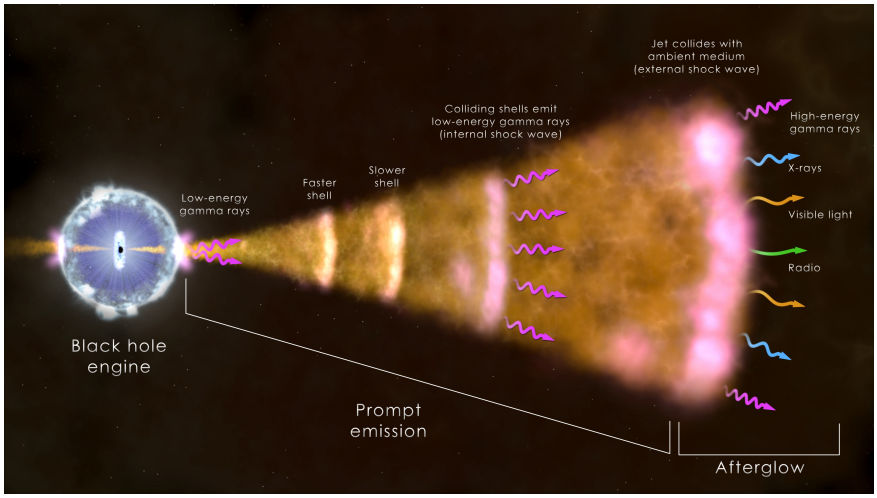

Figure 4.2. Schematic figure of a GRB jet, with the different emission mechanisms described in Sections 4.2.2, 4.2.3, and 4.2.4 shown. The various wavelength emission of the afterglow is also depicted. Figure adopted from NASA's Goddard Space Flight Center (2013).

times of $t_v \sim 10$ ms, unless the Lorentz factor of the outflow is extremely large. However, the theory of external shocks lead to the very important prediction of GRB afterglows (Rees & Mészáros, 1992), as we describe in more detail below in Section 4.3.

In Figure 4.2, a schematic ot a GRB jet is shown, indicating the different prompt emission possibilities outlined in this section.

4.3 Afterglow

The material surrounding the GRB explosion is called the circumburst medium. The GRB jet continuously drills through the circumburst medium as it propagates. Similarly to a snow plow, the circumburst material will be swept up this way. The circumburst medium is not very dense so the jet can reach large distances before it is affeted but in the end, inevitably, it has to slow down due to all the piled-up material.

The head of the jet creates a forward shock that pushes into the circumbursts medium. As explained in the sections on internal and external shocks (Sections 4.2.3 and 4.2.4 respectively), the shocks dissipates the kinetic energy of the outflow and converts it into internal energy in the downstream. The electrons in the downstream radiate this excess energy as synchrotron

radiation. When a large enough amount of material has been swept up, this synchrotron emission should be visible. Rees & Mészáros (1992) suggested this external shock radiation as an explanation for the prompt emission, which most people today believe it is not (although, see Burgess et al., 2016; Acuner et al., 2020). However, Rees & Mészáros (1992) also realized that even if it was not responsible for the prompt emission, it should nonetheless exist. Five years later, the afterglow emission was first observed (Costa et al., 1997).

The afterglow is a very important part of a GRB. First of all, it gave credit to the fireball model as the existence of the afterglow was predicted in the model before the observations were made. Apart from that, the afterglow has the advantage that it last much longer than the prompt emission. This makes the GRB easier to study with various other different detectors. For instance, optical information in the afterglow can give us the distance to the burst through redshift determination (see line emission in Section 2.3). The afterglow can also give us information regarding the total energy of the burst, the opening angle and the Lorentz factor of the outflow.

Once the jet has piled up enough material, it will start to decelerate. This means that the Lorentz factor of the outflow decreases, which has several consequences. One is that the emitted radiation becomes less Doppler boosted and the observed radiation is therefore less blueshifted. Thus, the observed spectrum will shift towards lower and lower energies. Another consequence of decreasing Lorentz factor is that the beaming becomes less significant. Recall (see Section 2.1) that most emission from a relativistically moving object is emitted into a solid cone of opening angle $\theta \sim 1/\Gamma$. With decreasing Γ, an observer is able to see emission from larger angles to her line of sight. Thus, the decrease in flux due to the decreasing Doppler boost is somewhat counteracted by an increase in flux as the observer is viewing a larger portion of the jet. At some point in the jet evolution however, $1/\Gamma$ will become larger than the jet opening angle. When this occurs, the observer is able to see emission from the whole jet at the same time. After this point, there is nothing to counteract the decrease due to lower Doppler boost and the flux will drop more rapidly in time. This is an important concept in afterglow theory called the *jet break*, due to the break it will create in the light curve. That GRB afterglows exhibit jet breaks indicates that the original outflow was collimated. From the jet break, the opening angle of the jet and whether the burst was viewed on or off axis can be deduced.

Chapter 5

Summary of attached papers

In this chapter, I will briefly summarize the main arguments and results of the two attached papers.

5.1 Paper I

We investigate whether high- or low-luminosity GRBs can be a major source of UHECRs. Paper I focuses on UHECR acceleration during the prompt phase. Two different scenarios are investigated with slightly different methodology. In the first scenario, the observed prompt spectrum is dominated by synchrotron emission, e.g., internal shocks (Section 4.2.3). In the second scenario, the prompt radiation is dominated by photospheric emission (Section 4.2.2).

In the synchrotron emission scenario, we use known properties of observed GRB photon spectra to constrain the possibility of UHECR acceleration. The νF_ν-peak energy $\varepsilon_{\rm peak}$ in the spectrum occurs at roughly $\sim$ 300 keV. In synchrotron models, the νF_ν-peak energy corresponds to $\varepsilon_{\rm peak} = \max[\varepsilon_{\rm m}, \varepsilon_{\rm c}]$, where $\varepsilon_{\rm m}$ and $\varepsilon_{\rm c}$ are the characteristic energies of photons emitted by electrons with the characteristic Lorentz factor $\gamma'_{\rm m}$ and $\gamma'_{\rm c}$ respectively. Here, $\gamma'_{\rm m}$ and $\gamma'_{\rm c}$ are the injection and cooling Lorentz factor as described in Section 2.5.3). To account for acceleration up to the highest UHECR energies observed, the GRBs are required to have quite high magnetic fields strengths. The electrons subjected to these high magnetic fields quickly lose their energy due to synchrotron radiation, which decreases $\gamma'_{\rm c}$. Small values of $\gamma'_{\rm c}$ results in small values of $\varepsilon_{\rm c}$. Indeed, for all the parameter

space that would allow for UHECR acceleration, $\varepsilon_{\rm c} \ll \varepsilon_{\rm peak}$, which implies that $\varepsilon_{\rm m} = \varepsilon_{\rm peak}$ and that the electrons are very fast cooling. However, this is in tension with observations that suggest observed GRB spectra to be at most marginally fast cooling with $\gamma'_{\rm c} \lesssim \gamma'_{\rm m}$ (Section 4.2.3).

If the observed spectrum is photospheric, then we have to use a different argument. It is still true that the magnetic fields need to be high to account for UHECR acceleration and that the co-accelerated electrons emit synchrotron radiation in this magnetic field. However, in this scenario the observed spectrum is not from the accelerated electrons, thus we cannot assign $\varepsilon_{\rm m} = \varepsilon_{\rm peak}$. Instead, we use the constraint that the emitted synchrotron radiation must be subdominant to the observed spectrum. If it is not, then we can refer back to the previous argument of synchrotron dominated prompt emission. In other words, in the previous scenario we used the *shape* of the observed photon spectrum to constrain UHECR acceleration while here we use the overall *normalization*. We found that the synchrotron radiation emitted by the co-accelerated electrons would be orders of magnitude higher than typical GRB fluxes, specifically in optical frequencies. The high magnetic fields needed for UHER acceleration results in very rapid energy losses for the electrons, producing a high flux. This result was valid for both high and low-luminosity GRBs.

Lastly, we investigated the parameter dependence of the results in Paper I. We found that if GRBs are responsible for UHECR acceleration, then it is necessary that only a small fraction of the available electrons are accelerated. Furthermore, this small number fraction should receive a small portion of the energy in order to be consistent with observations. We suggested that high optical flux could be an indicative signature of successful UHECR acceleration.

5.2 Paper II

Following on Paper I, Paper II applies the same methodology to the specific low-luminosity GRB 060218. An advantage of considering this specific GRB is that there exist very good data in several different energy bands. Therefore, where we in Paper I assumed typical fluxes applicable to the whole GRB sample, in Paper II we can compare the predictions to direct measurements. Furthermore, Paper I extends on the work in Paper II by considering acceleration of UHECR during the afterglow phase as well.

For the prompt phase we use the same methodology as for the photospheric models in Paper I. Indeed, that the produced flux from the co-accelerated electrons cannot be brighter than the observation is true regardless of the prompt emission model. The results for GRB 060218 are similar but much stronger to those presented for llGRBs in Paper I. The results are

stronger because the optical measurement of GRB 060218 is much lower than the optical flux limit we used for llGRBs in Paper I.

For the afterglow phase we considered a different method. The method for the afterglow is similar to that of the prompt as both compare the predicted emission from the co-accelerated electrons with observation to constrain the possibility of UHECR acceleration. However, for the afterglow phase, we used the fact that the afterglow blast wave has to contain the required minimum energy to supply the observed flux of UHECR at Earth, as described in Section 3.5. This energy was much higher than previous estimates of the afterglow energy in GRB 060218. This forced us to consider a composite model for the electron distribution, where a fraction ξ_a of the electrons are accelerated into a power-law while the rest $(1-\xi_a)$ are thermal. With the thermal electrons included, the total energy of the blast wave can be constrained.

We found that the thermal electrons radiate mostly in the radio band. Comparing the emission from the these electrons to the radio data at $\sim$ 3 days, we found that the parameters necessary to be consistent with the radio data are disfavored by particle-in-cell simulations. However, if the energy of the blast wave was reduced, we found that the radio data could be satisfied with parameter values in line with predictions. We concluded that the afterglow phase of GRB 060218 likely did not have sufficient energy to be a major source of UHECRs. Lastly, we argued that because GRB 060218 seemed comparable to other llGRBs in terms of prompt optical flux and afterglow radio flux, these result might extend to the whole llGRB population.

Acknowledgments

I would like to thank my supervisor Felix Ryde, and Damien Bégué for their continuous supervision and support. A special thanks to Asaf Pe'er for his supervision during my time at Bar-Ilan University. I also thank all my friends and colleagues at the Particle and Astroparticle Physics department. Lastly I thank, my partner Angelica Alamaa, my family, and my friends for brightening my life outside of working hours.

Bibliography

Abbott B. P., et al., 2016, PRL, 116, 061102

Abbott B. P., et al., 2017a, PRL, 119, 161101

Abbott B. P., et al., 2017b, ApJL, 848, L12

Abraham J., et al., 2004, Nuclear Instruments and Methods in Physics Research A, 523, 50

Abramowicz M. A., Novikov I. D., Paczynski B., 1991, ApJ, 369, 175

Acuner Z., Ryde F., Pe'er A., Mortlock D., Ahlgren B., 2020, ApJ, 893, 128

Arnett W. D., Bahcall J. N., Kirshner R. P., Woosley S. E., 1989, ARAA, 27, 629

Baerwald P., Bustamante M., Winter W., 2013, ApJ, 768, 186

Band D., et al., 1993, ApJ, 413, 281

Bell A. R., 1978, MNRAS, 182, 147

Beloborodov A. M., 2010, MNRAS, 407, 1033

Biehl D., Boncioli D., Lunardini C., Winter W., 2017, preprint, (arXiv:1711.03555)

Blumenthal G. R., Gould R. J., 1970, Reviews of Modern Physics, 42, 237

Boncioli D., Biehl D., Winter W., 2019, ApJ, 872, 110

Burgess J. M., Bégué D., Ryde F., Omodei N., Pe'er A., Racusin J. L., Cucchiara A., 2016, ApJ, 822, 63

Burgess J. M., Bégué D., Bacelj A., Giannios D., Berlato F., Greiner J., 2018, arXiv e-prints,

Bustamante M., Heinze J., Murase K., Winter W., 2017, ApJ, 837, 33

Campana S., et al., 2006, Nature, 442, 1008

Caprioli D., Spitkovsky A., 2014, ApJ, 794, 47

Costa E., et al., 1997, Nature, 387, 783

D'Elia V., et al., 2018, A&A, 619, A66

Daigne F., Bošnjak Ž., Dubus G., 2011, A&A, 526, A110

Einstein A., 1905a, Annalen der Physik, 322, 549

Einstein A., 1905b, Annalen der Physik, 322, 891

Einstein A., 1915, Sitzungsberichte der Königlich Preußischen Akademie der Wissenschaften (Berlin, pp 844–847

Fan Y.-Z., Piran T., Xu D., 2006, JCAP, 9, 013

Fermi E., 1949, Physical Review, 75, 1169

Fishman G. J., et al., 1994, ApJS, 92, 229

Galama T. J., et al., 1998, Nature, 395, 670

Ghisellini G., et al., 2020, A&A, 636, A82

Goodman J., 1986, ApJL, 308, L47

Greisen K., 1966, PRL, 16, 748

Guetta D., Della Valle M., 2007, ApJL, 657, L73

Harris R., 2008, Modern Physics. Pearson/Addison-Wesley

Heinze J., Fedynitch A., Boncioli D., Winter W., 2019, ApJ, 873, 88

Hess V. F., 1912, Physikalische Zeitschrschift, 13, 1084

Hillas A. M., 1984, ARAA, 22, 425

Hjorth J., et al., 2003, Nature, 423, 847

Hugoniot H., 1887a, Journal de l'École Polytechnique, 57, 3

Hugoniot H., 1887b, Journal de l'École Polytechnique, 58, 1

Hümmer S., Rüger M., Spanier F., Winter W., 2010, ApJ, 721, 630

IceCube Collaboration 2013, Science, 342, 1242856

IceCube Collaboration 2020, GRB Coordinates Network, 26655, 1

IceCube Collaboration et al., 2018a, Science, 361, 147

IceCube Collaboration et al., 2018b, Science, 361, eaat1378

Katz B., Budnik R., Waxman E., 2009, JCAP, 3, 020

Keivani A., et al., 2018, preprint, (arXiv:1807.04537)

Kouveliotou C., Meegan C. A., Fishman G. J., Bhat N. P., Briggs M. S., Koshut T. M., Paciesas W. S., Pendleton G. N., 1993, ApJL, 413, L101

Lazzati D., Morsony B. J., Margutti R., Begelman M. C., 2013, ApJ, 765, 103

Lundman C., Pe'er A., Ryde F., 2013, MNRAS, 428, 2430

Mészáros P., 2006, Reports on Progress in Physics, 69, 2259

Mészáros P., Fox D. B., Hanna C., Murase K., 2019, Nature Reviews Physics, 1, 585

Mücke A., Rachen J. P., Engel R., Protheroe R. J., Stanev T., 1999, PASA, 16, 160

Murase K., Takami H., 2009, ApJL, 690, L14

Murase K., Ioka K., Nagataki S., Nakamura T., 2008, PRD, 78, 023005

NASA Science Official 2019, The Burst And Transient Source Experiment, https://heasarc.gsfc.nasa.gov/docs/cgro/batse/

NASA's Goddard Space Flight Center 2013, NASA Sees 'Watershed' Cosmic Blast in Unique Detail, https://www.nasa.gov/content/goddard/nasa-sees-watershed-cosmic-blast-in-unique-detail

Nakar E., Sari R., 2012, ApJ, 747, 88

National Science Foundation 2018, NSF Press Conference on Breakthrough in Multi-messenger Astrophysics, https://www.youtube.com/watch?v=iChBhHpFtMI

Nobel Media AB 2002, Two New Windows on the Universe, https://www.nobelprize.org/prizes/physics/2002/press-release/

Nobel Media AB 2017, Gravitational waves finally captured, https://www.nobelprize.org/prizes/physics/2017/press-release/

Oganesyan G., Nava L., Ghirlanda G., Melandri A., Celotti A., 2019, A&A, 628, A59

Paczyński B., 1986, ApJL, 308, L43

Pe'er A., 2008, ApJ, 682, 463

Pe'er A., 2015, Advances in Astronomy, 2015, 907321

Pian E., et al., 2006, Nature, 442, 1011

Pinfold J., Atlas Collaboration 2017, in European Physical Journal Web of Conferences. p. 10001, doi:10.1051/epjconf/201714510001

Preece R. D., Briggs M. S., Mallozzi R. S., Pendleton G. N., Paciesas W. S., Band D. L., 1998, ApJL, 506, L23

Protheroe R. J., Clay R. W., 2004, PASA, 21, 1

Rankine W. J. M., 1870, Phil. Trans. R. Soc., 160

Ravasio M. E., Oganesyan G., Ghirlanda G., Nava L., Ghisellini G., Pescalli A., Celotti A., 2018, A&A, 613, A16

Ravasio M. E., Ghirlanda G., Nava L., Ghisellini G., 2019, A&A, 625, A60

Rees M. J., Mészáros P., 1992, MNRAS, 258, 41P

Rees M. J., Mészáros P., 1994, ApJL, 430, L93

Rees M. J., Mészáros P., 2005, ApJ, 628, 847

Rieger F. M., Bosch-Ramon V., Duffy P., 2007, ApSS , 309, 119

Ruderman M., 1975, in Bergman P. G., Fenyves E. J., Motz L., eds, Seventh Texas Symposium on Relativistic Astrophysics Vol. 262, Seventh Texas Symposium on Relativistic Astrophysics. pp 164–180, doi:10.1111/j.1749-6632.1975.tb31430.x

Rybicki G. B., Lightman A. P., 1979, Radiative processes in astrophysics. John Wiley & Sons, Inc

Ryde F., et al., 2010, ApJL, 709, L172

Ryde F., Lundman C., Acuner Z., 2017, MNRAS, 472, 1897

Sari R., Piran T., Narayan R., 1998, ApJL, 497, L17

Sazonov S. Y., Lutovinov A. A., Sunyaev R. A., 2004, Nature, 430, 646

Schilling G., 2002, Flash! The hunt for the biggest explosions in the universe.. Cambridge University Press

Schmidt W. K. H., 1978, Nature, 271, 525

Soderberg A. M., et al., 2006, Nature, 442, 1014

Starling R. L. C., et al., 2011, MNRAS, 411, 2792

Sun H., Zhang B., Li Z., 2015, ApJ, 812, 33

The Pierre Auger Collaboration et al., 2015, arXiv e-prints, p. arXiv:1509.03732

Toma K., Ioka K., Sakamoto T., Nakamura T., 2007, ApJ, 659, 1420

Treumann R. A., Jaroschek C. H., 2008, arXiv e-prints, p. arXiv:0805.2162

Waxman E., 1995a, Physical Review Letters, 75, 386

Waxman E., 1995b, ApJL, 452, L1

Waxman E., Mészáros P., Campana S., 2007, ApJ, 667, 351

Wulf T., 1910, Physikalische Zeitschrschift, 11, 811

Zatsepin G. T., Kuz'min V. A., 1966, Soviet Journal of Experimental and Theoretical Physics Letters, 4, 78

Zhang B. T., Murase K., Kimura S. S., Horiuchi S., Mészáros P., 2018, PRD, 97, 083010